



CARACTERIZACIÓN DE RESIDUOS ALCALINOS GENERADOS EN LA INDUSTRIA DEL ALUMINIO PARA SU USO EN LA DESCONTAMINACIÓN DE LIXIVIADOS ÁCIDOS

Luciana Badano Patiño

Trabajo entregado para la obtención del grado de Master en Tecnología
Ambiental

Modalidad: Investigación

Diciembre / 2022

Directores:

Dr. Juan Pedro Bolívar Raya
Dra. Silvia M. Pérez Moreno

Dr. Juan Pedro Bolívar Raya, DNI: 30451377K, cargo Director de RENSMA y Dra. Silvia Pérez Moreno, DNI: 44203353K y cargo Investigador Postdoctoral, en el departamento de Ciencias Integradas de la entidad Universidad de Huelva,

INFORMAN:

Que el trabajo titulado “Caracterización de residuos alcalinos generados en la industria del aluminio para la descontaminación de lixiviados ácidos.” presentado por Da. Luciana Badano Patiño, con D.N.I.: Y9129146T, ha sido realizado en “Departamento de Ciencias Integradas”, bajo mi dirección, y autorizo su presentación y defensa como Trabajo Fin de Máster (Modalidad: Investigación), para el Máster Universitario en Tecnología Ambiental de la Universidad de Huelva.

En Huelva, a 7 de diciembre de 2022

Fdo.: Juan Pedro Bolívar Raya - Silvia Pérez Moreno

RESUMEN

Sobre las marismas del río Tinto (Huelva, España), se han depositado aproximadamente 100 Mt de fosfoyeso, un residuo de la industria del ácido fosfórico que estuvo operativa por 42 años en esta ciudad, cerrándose el 31/12/2010. A partir de estos depósitos y de su interacción con el medio, se generan lixiviados altamente ácidos ($\text{pH} = 1-2$) que contienen altas concentraciones de metales pesados y radionucleidos (entre 2 y 4 órdenes de magnitud mayores que el agua de mar), que escapan desde las pilas hacia el estuario del río Tinto. En el presente no se realiza ningún tratamiento a estos lixiviados previo a su vertido en el estuario, lo cual supone un alto riesgo medioambiental.

En este trabajo se caracterizaron residuos de la industria del aluminio (red mud) provenientes de dos orígenes (RM-H y RM-P) además de un residuo proveniente de la combustión de biomasa (ceniza doméstica) para su posible aplicación en la descontaminación de lixiviados de fosfoyeso (PGL). Sus propiedades alcalinas se analizaron mediante curvas de titulación de las cuales se obtuvo la capacidad de neutralización de ácidos (ANC), el máximo pH que puede alcanzarse con cada residuo y la relación sólido líquido necesaria para esto. Las fases líquidas resultantes se estudiaron para conocer la calidad del efluente obtenido y verificar su cumplimiento con las normas de vertido. Estos resultados mostraron que las cenizas tienen mayor ANC que los red mud y que los dos red mud estudiados presentan ANC muy similares con los tres ácidos estudiados (HNO_3 , H_3PO_4 y PGL). Los tres residuos fueron capaces de neutralizar el PGL hasta $\text{pH} = 7$, siendo las cenizas las que requieren menor cantidad para lograrlo, seguidas de RM-H y RM-P. La calidad del líquido final muestra una alta reducción de todos los contaminantes, a excepción del As, luego del contacto con el sólido, lo que implica que los residuos tienen potencial para su utilización como agentes alcalinos en un tratamiento pasivo del lixiviado.

Además, se realizaron experimentos batch para el estudio del coeficiente de partición (K_d) de los principales contaminantes con red mud. A partir de estos resultados, dos de los contaminantes estudiados pudieron ajustarse a los modelos de isoterma de adsorción de Freundlich (Ni) y Dubinin-Radushkevich (Cd y Ni).

ABSTRACT

Approximately 100 Mt of phosphogypsum have been deposited on the Tinto river marshes (Huelva, Spain), this residue came from the phosphoric acid industry that operated for 42 years in this city, closing on 12/31/2010. From these deposits and their interaction with the environment, highly acid leachates ($\text{pH} = 1\text{-}2$) are generated, they contain high concentrations of heavy metals and radionuclides (between 2 and 4 orders of magnitude greater than seawater) and escape from the piles towards the estuary of the Tinto river. At present, no treatment is applied to these leachates prior to their discharge into the estuary, which implies a high environmental risk.

In this work, residues from the aluminum industry (red mud) from two sources were characterized, in addition to a residue from the combustion of biomass (domestic ash) for their possible application in decontamination of phosphogypsum leachates (PGL). Their alkaline properties were analyzed by titration curves from which the acid neutralization capacity (ANC), the maximum pH that can be reached with each residue and the solid-liquid ratio necessary to achieve it were determined. The resulting liquid phases were studied to find out the quality of the effluent obtained and verify its compliance with estuary discharge regulations. These results showed that ashes have higher ANC than red mud and that the two studied red muds present very similar ANC with the three acids studied (HNO_3 , H_3PO_4 y PGL). The three residues were able to neutralize the PGL up to $\text{pH} = 7$, being the ashes the ones that require the least quantity to achieve it, followed by RM-H and RM-P. The quality of the final liquid shows a high reduction of all contaminants, with the exception of As, after contact with the solid, which implies that the residues have the potential to be used as alkaline agents in a passive treatment of the leachate.

In addition, batch experiments were carried out to study the partition coefficient (K_d) of the main pollutants with red mud. Based on these results, two of the pollutants studied could be fitted to the Freundlich (Ni) and Dubinin-Radushkevich (Cd and Ni) adsorption isotherm models.

Content

1	Introduction	12
1.1	Problem to solve	12
1.2	Fundamental concepts	14
1.3	State of the art	21
1.4	Objectives	25
2	Materials and methods	26
2.1	Samples and materials	26
2.2	Pre-treatment	28
2.3	Analytical techniques	30
2.3.1	Alpha spectrometry	30
2.3.2	Inductively coupled plasma optical emission spectrometry (ICP-OES)	32
2.3.3	Inductively coupled plasma mass spectrometry (ICP-MS)	32
2.3.4	Ion Chromatography	33
2.3.5	X-Ray Fluorescence (XRF)	33
2.3.6	X-Ray Diffraction (XRD)	34
2.3.7	Quality control	34
2.4	Design of experiments	36
2.4.1	Titration curves	36
2.4.2	Batch experiments	38
3	Results and discussion	41
3.1	PGL characterization	41
3.2	Solid waste characterization	45
3.3	Study of the acid neutralization capacity of solids	53
3.3.1	Titration curves	53
3.3.2	Removal of contaminants in titration curves	60
3.4	Batch Experiments	64
3.4.1	Batch experiment 1	64
3.4.2	Batch experiment 2	76
4	Conclusions	79
	Appendix	89
A	Quality control	89
B	Solid wastes characterization	91
C	Isotherm adsorption models	92

List of Figures

1.1	Location and zones of the Huelva phosphogypsum stacks.	14
1.2	Adsorption isotherm models shapes.	20
2.1	Scheme of the bayer process for alumina production.	27
2.2	Solid waste materials studied.	28
2.3	Solid residues pre-treatment.	30
2.4	Comparison of major elements composition of the solids obtained by analysis of ICP-OES and XRF.	36
2.5	Experiment setup for titration curves.	38
2.6	Batch experiments.	40
3.1	Scheme of a titration curve of a diprotic acid with a strong base. Extracted from <i>Titration of a Weak Polyprotic Acid</i> , 2022, LibreText Chemistry (https://chem.libretexts.org).	44
3.2	Titration curve of PGL with NaOH 1.5 M, circles symbolize midpoints and crosses equivalence points.	45
3.3	Fractions of each solid residue obtained after sieving.	47
3.4	Solid waste mayor elements and typical soil (TS) composition values. LOI: loss on ignition.	49
3.5	Solid waste trace elements composition, NGR and typical soil (TS) composition values.	49
3.6	Diffraction patterns of the solid wastes.	51
3.7	Titration curves for RM-H, RM-P and DA with HNO ₃ 0.55 M (RM-H and RM-P) 1.1 M (DA). Circles represent midpoints and crosses equivalence points.	55
3.8	Titration curves for RM-H, RM-P and DA with H ₃ PO ₄ 0.5 M and PGL.	58
3.9	pH variation in Batch experiments 1A and 1B.	66
3.10	Effect of initial adsorbate concentration (C_0) and amount of solid on the final concentration (C_d) of contaminants from aqueous solution by the RM-H. The dashed line represents $C_d=C_0$	67
3.11	Effect of initial adsorbate concentration (C_0) and amount of solid on the final concentration (C_d) of contaminants from aqueous solution by the RM-P. The dashed line represents $C_d=C_0$	68
3.12	Effect of initial adsorbate concentration on the removal of contaminants from aqueous solution by the RM-H.	72
3.13	Effect of initial adsorbate concentration on the removal of contaminants from aqueous solution by the RM-P.	73
3.14	Linear fit of Ni and Cd isotherms to Freundlich model (a and c) and DR model (b and d).	75

3.15	pH variation with time in Batch experiment 2A with $DF=1/100$	77
3.16	pH variation with time in Batch experiment 2B with $DF=1/10$	78
C.1	Best fit of Ni and Cd isotherms to Freundlich model (a abd c) and DR model (b and d).	92

List of Tables

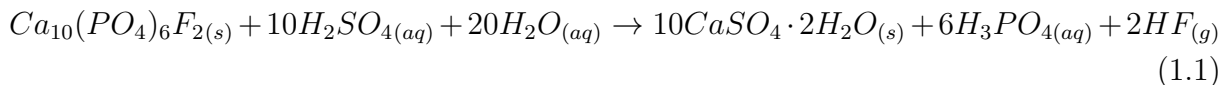
2.1	Waste materials used and their corresponding numerical and alphabetic codes.	28
2.2	Parameters and R^2 of the linear fits of XRF vs ICP-OES for the three studied solid wastes. Standard uncertainties are given.	36
2.3	Variables of Batch experiments. Dissolution volume = 150 mL. Agitation = 230 rpm. S/L = solid to liquid mass ratio, DF = Dilution Factor ($C_0 = C_{0i} \cdot DF$, C_{0i} : original PGL concentration).	39
3.1	Composition of PGL measured by ICP-OES, ICP-MS, ion chromatography and alpha spectrometry, background values and emission limits established by Decreto 109/2015 (2015).	42
3.2	Solid waste characterization	45
3.3	Solid waste granulometry (%).	46
3.4	Mineral and amorphous phases identified and quantified in the solids by XRD in %.	52
3.5	Comparison of results of HNO_3 , H_3PO_4 and PGL titration curves with the different solids. $m_{dissolution} = 150$ g, S/L = Solid to liquid ratio for final pH.	57
3.6	Solid wastes acid neutralization capacity (ANC) of a strong and a weak acid in molar mili Equivalents / g of residue for pH=7.	57
3.7	Initial concentration, emission limit established by Decreto 109/2015 2015, final concentration, and removal efficiency of studied elements in PGL titration curves with solids. Red indicates values above emission limit, blue indicates RE < 90 %.	63
3.8	pH results of Batch experiments 1A (S/L = 1/3.75) and 1B (S/L = 1/7.50).	65
3.9	Parameters of the best fit model of the Cd and Ni isotherms with RM-H and RM-P.	76
A.1	Quality control of ICP-MS analysis in laboratories CIC (Granada) and CIDERTA (Huelva). Relative differences of the measured concentrations and the standard concentrations.	89
A.2	Quality control of ICP-OES analysis in laboratories CIC (Granada) and CIDERTA (Huelva). Relative differences of the measured concentrations and the standard concentrations.	89
A.3	Quality control of XRF analysis results from laboratory CITIUS (Seville) by comparison with ICP-OES results from CIC (Granada).	90
B.1	Solid residues composition of mayor elements (%) and trace elements (mg/kg), measured by XRF, ICP-OES and and ICP-M, typical soil values and NGR values.	91

1 Introduction

1.1 Problem to solve

In Huelva (SW of Spain), phosphoric acid production industry took place from 1968 to 2010 and its plants were located in the vicinity of the estuary formed by the confluence of the Tinto and Odiel rivers.

Phosphoric acid production is based on the dissolution of the raw material, called “Phosphate Rock” (PR), being fluorapatite the most used one in Huelva, by adding diluted sulphuric acid (70 %). This generates phosphoric acid (PA) and a white solid named phosphogypsum (PG) (Equation 1.1), of which more than 95 % is calcium sulfate dihydrate ($\text{CaSO}_4 \cdot 2\text{H}_2\text{O}$) (Bolivar et al. 1996). The solid fraction is separated from the acid through filtration, and then washed several times to recover almost all the remaining phosphoric acid contained in the PG (more than 95 %), and finally, it is sent by pumping into piles for storage. Hydrogen fluoride gas is also produced in this process and sent to scrubbers where it is absorbed into water, producing a weak hydrofluoric acid effluent, which is mixed with phosphogypsum and deposited with it in the storage piles.



The phosphate industry is classified as a NORM (Naturally Occurring Radioactive Material) activity, since the raw material often contains natural radionuclides activity concentrations higher than the established thresholds by the EU Directives (European Parliament 2014) and the Spanish regulation (BOE 2001, CSN 2011), and therefore the phosphogypsum stacks entail a radiological and environmental problem.

The PR used in Huelva is very enriched in ^{238}U and daughters, with concentrations about 50 times higher than typical soils, while the concentrations of ^{40}K , ^{228}Th and daughters are lower or similar as in typical soils (Bolivar et al. 1996). In previous studies (Bolivar et al. 2009), it was estimated that more than 95% of the total Ra, Pb, Th, and ^{210}Po contained in the PR is transferred to the PG, whereas the U is transferred in less quantity, between 5 % and 20 %.

For every ton of P_2O_5 produced as phosphoric acid, 4.5–5.5 tons of dry mass of phosphogypsum is produced (IAEA 2013). Annually, about $2.5 \cdot 10^6$ tons of phosphogypsum were generated in the industries of Huelva as a residue of phosphoric acid production. The PG was managed in different ways in Huelva according to two periods: from 1968 to 1997, 20 % of PG was directly pumped with seawater into the Odiel estuary, and the remaining 80 % was pumped in suspension (20 % PG and 80 % seawater) into stacks located in the Tinto estuary saltmarshes, where PG was decanted and the used seawater,

with pH around 2 and high concentrations of pollutants, was released into Tinto estuary without any treatment (Bolivar et al. 1996). From 1998 to 2010, the management system changed, the pumping was done with freshwater into the zone 2 of stacks, and after PG decantation, the used water was returned into the phosphoric acid plants. This managed to reduce pollutant emissions from PG stacks to the estuary in more than 95 % (Absi et al. 2004). On December 2010 the production of PA in Huelva stopped by a resolution of the Supreme Court of Spain.

According to Mas et al. (2006), approximately 100 Mt of PG are stored in the piles that occupy an area of 1000 ha and are located very close to the city of Huelva (Figure 1.1). Since 1990, several restoration works have been developed at the phosphogypsum piles. The area is divided in 4 zones, having the zones 1, 3 and 4 a mean height of 5 m, while the zone 2 has a pyramidal shape with 20 m height. Zone 1 was the first one to be restored and revegetated in 1990-92 by using a soil layer of 40 cm, while zone 4 was remediated between 1997 and 2009 by the governments of Huelva city and Andalusia region. There is currently a project from the company Fertiberia that has been partially approved, for the restoration of zones 2 and 3, which are to date unrestored and therefore still exposed to environmental weathering. These two piles are surrounded by a series of perimeter channels where the leachates from PG weathering are collected, but this effluent is discharged uncontrollably to the estuarine environment through edge leakages (Papaslioti et al. 2018b, Pérez-López et al. 2016), which makes it of most importance for a treatment of these leachates to be implemented.

The restoration project consists in covering the PG surface of zones 2 and 3 with a geomembrane, followed of a compacted clay layer (60 cm), a drainage layer of coarse material, and finishing with a revegetated soil layer of about 1 m thick. It also includes a perimeter channel to collect the lateral leachates outflows that are expected to continue to occur.



Figure 1.1: Location and zones of the Huelva phosphogypsum stacks.

Since 2020, the FRYMA group (Radiation Physics and Environment) of the University of Huelva has been working on a project called “Development and optimization of a process for removing natural radionuclides in leachates from phosphogypsum, and valorization of the generated wastes”. One of the main objectives of this project is to develop and optimize a chemical process at laboratory scale for removing the natural radionuclides and potential toxic elements from the leachates of the PG. This objective can be achieved in two different ways: active and passive methods.

1.2 Fundamental concepts

A passive treatment is one in which the effluent passes through a solid medium (called a permeable reactive barrier, PRB) which is composed of a mixture of an inert material

and a reactive material capable of removing the desired contaminants by retaining or transforming them through physical, chemical and biological processes to improve the quality of the water (Kumarasinghe et al. 2018). This generally requires a relatively small amount of energy and materials once in operation since its functioning is based on the flow of water by gravity. Passive systems have the advantage of being self-sufficient with sporadic maintenance, very low capital and operating costs, but the quality of the final effluent is often not as good as the one obtained with an active treatment. Although passive treatment approaches are economically attractive, they have some limitations. For example, the lifespan of a barrier is related to the removing processes of compounds, that cause the decrease over time of its porosity, hydraulic conductivity as well as the reactive surface of the reactive material, which causes a continuous decrease in efficiency (Macián 2007). Prior to the design and installation of a PRB, it is necessary to characterize the reactive medium and its interaction with the pollutants to be removed.

In active treatments, the water is treated in a controlled process, where a continuous supply of resources is often required to sustain said process. Although the operating costs and initial investment may be higher, the quality of the effluent is very high, with some potential for cost recovery through the sale of water, metals and by-products, so this can be considered a great advantage over passive treatments. On the other hand, they require the use of chemicals, operation and maintenance personnel, and electrical power to function efficiently.

To understand the functioning of a PRB, it is necessary to take into account the main chemical interactions that occur between dissolved and particulate matter, these are: complexation, oxidation-reduction, and sorption. Within sorption are the mechanisms of dissolution-precipitation, adsorption-desorption, absorption and partitioning in organic matter. Dissolution-precipitation and adsorption-desorption are considered the most important processes affecting the interaction of metals and radionuclides with soils, while precipitation is particularly important for the behavior of heavy metals (EPA 1999). Adsorption is defined as the accumulation of matter at the interface between a solid phase and an aqueous solution phase. The matter that accumulates in 2-dimensional molecular arrangements at the interface is defined as the adsorbate and the solid surface on which it accumulates is the adsorbent.

So, sorption is a general term used to describe the partitioning of the constituents of the aqueous phase into a solid phase and the partition (or distribution) coefficient (K_d) is a value frequently used to quantify sorption. K_d is defined as the ratio between the adsorbate concentration in the solid phase per unit mass of solid and the concentration that remains in solution at equilibrium, in units of mL/g:

$$k_d = \frac{C_s}{C_d} \quad (1.2)$$

- C_s : Contaminant concentration in the solid material (mg/g of solid)
- C_d : Contaminant concentration in the dissolution phase (mg/L)

The value of K_d varies according to the chemical element, the characteristics of the aqueous phase and the solid, both physical (such as the specific surface) and chemical, in addition to the conditions of the medium such as pH, Eh and temperature. In particular, the magnitude and polarity of the net surface charge of a mineral changes with pH and changes from positive to negative at the point of zero charge (pH_{ZPC}), so at $\text{pH} < \text{pH}_{ZPC}$ the solids surface has net positive charge which favors adsorption of contaminants present as dissolved anions, and a $\text{pH} > \text{pH}_{ZPC}$, results in a net negative-charge which favors adsorption of contaminants present as dissolved cations.

K_d models

There are several possible models to describe sorption according to the behavior of K_d . The most used ones are (EPA 1999):

1. Constant K_d Model
2. Parametric K_d Model
3. Isotherm Adsorption Models

In the first model, the value of K_d is considered to be constant, this implies assuming that the unoccupied surface adsorption sites are much larger than the total dissolved adsorbate in solution, that is, the solid cannot become saturated. A limitation of this model is that it is only valid for the conditions in which it was measured, it does not address sensitivity to changing environmental conditions. If the properties of the liquid phase (e.g., pH, ionic strength of the solution or adsorbate concentration) change, a different K_d value should be used in the model.

Parametric K_d model considers that K_d value varies as a function of empirically derived relationships with aqueous and solid phase independent parameters. It is more robust than the constant K_d model and removes the work of determining new K_d values for each environmental condition. The empirical predictor equations commonly take the form of a nonlinear polynomial expression. A disadvantage of this model is that these types of statistical relationships provide no certain information on the mechanism by which the radionuclide or heavy metal partitioned to the solid phase, whether it be by adsorption, absorption, or precipitation.

Adsorption isotherms arise from the results of a set of experiments evaluating the effect of

contaminant concentration on adsorption, while holding other parameters constant. They are physicochemical models that consider hypotheses about the adsorption/desorption mechanisms, and therefore are useful to analyze which of them are the predominant ones in a given adsorbent and medium. These models are used to describe the case where sorption ratios deviate from linearity, which is common to happen in soils. For many short-lived radionuclides, the mass present never reaches large enough amounts to start charging the surface adsorption sites to the point that the K_d relationship is no longer linear. However, long-lived radionuclides and stable elements can be found in leachates and groundwater near waste sources in concentrations large enough to affect the saturation of surface adsorption sites (EPA 1999). The most commonly used adsorption isotherm models are the Langmuir, Freundlich, and Dubinin-Radushkevich models.

The Langmuir model (Langmuir 1919) was originally proposed to describe the adsorption of gas molecules on homogeneous solid surfaces. Many researchers have extended the Langmuir adsorption model to describe the adsorption of species in solution on solid adsorbents, including heterogeneous solids such as soils. Basic assumption of Langmuir isotherm is that adsorption takes place at specific homogeneous sites within the adsorbent (Günay et al. 2007), and it is described by:

$$C_s = \frac{K_L C_m C_d}{1 + K_L C_d} \quad (1.3)$$

where

- C_s : amount of adsorbate adsorbed per unit mass of solid (mg/g)
- K_L : Langmuir adsorption constant related to the energy of adsorption (L/mg)
- C_m : maximum adsorption capacity of the solid (mg/g)
- C_d : equilibrium solution concentration of the adsorbate (mg/L)

Equation 1.3 can be linearized by changing the variable $B=1/K_L$ to obtain:

$$C_s = -B \frac{C_s}{C_d} + C_m \quad (1.4)$$

This allows to obtain the value of the constant K_L from the slope of the best linear fit of the plot C_s vs C_s/C_d and the value of C_m from the interception.

Freundlich isotherm model assumes heterogeneous surface with a nonuniform distribution of heat of adsorption (Günay et al. 2007) and is mathematically expressed as (Freundlich 1926):

$$C_s = K_F C_d^N \quad (1.5)$$

where

- C_s : amount of adsorbate adsorbed per unit mass of solid (mg/g)
- C_d : equilibrium solution concentration of the adsorbate (mg/L)
- K_F : Freundlich adsorption constant (mg/g)
- N : constant

This relationship does not take into account the finite adsorption capacity at high solute concentrations, but when studying trace constituents, it is usually not significant to ignore this physical limitation. When $N=1$, the Freundlich isotherm reduces to a linear relationship and $K_F=K_d$. That is, constant K_d is a particular case of the Freundlich model. Equation 1.5 can be linearized by taking the logarithm of both sides:

$$\log C_s = \log K_F + N \cdot \log C_d \quad (1.6)$$

Thus, using the linear fit of the plot $\log C_s$ vs $\log C_d$, the values of K_F and N can be obtained from the interception and the slope, respectively. This model applies well to many radionuclides where the value of N is often significantly different from 1. Sposito (1984) determined that the Freundlich isotherm only applies to data obtained at low values of C_d .

Finally, the Dubinin-Radushkevich isotherm is applied to find out the adsorption mechanisms based on the potential theory assuming heterogeneous surface (Dabrowski 2001) and it is expressed as (Dubinin 1947):

$$C_s = C_m e^{-K_D \epsilon^2} \quad (1.7)$$

where

- C_s : amount of adsorbate adsorbed per unit mass of solid (mg/g)
- C_m : sorption capacity of adsorbent per unit mass (mg/g)
- K_D : Dubinin-Radushkevich adsorption constant (mol^2/kJ^2)
- ϵ : $RT \ln(1 + 1/C_d)$
- R : gas constant (8.314 J/mol·K)
- T : temperature (K)

- C_d : equilibrium solution concentration of the adsorbate (mg/L)

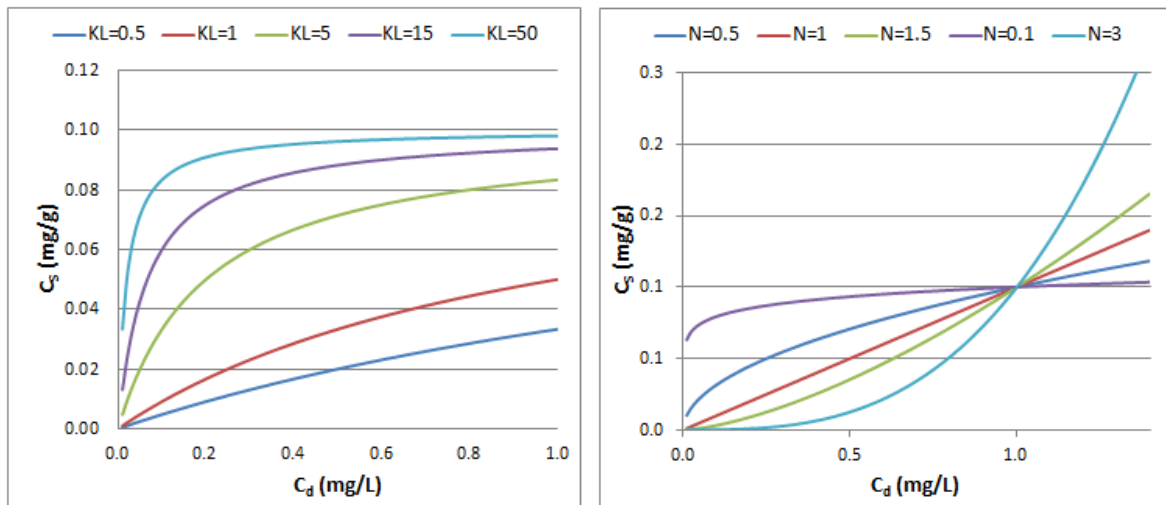
This model has often successfully fitted high solute activities (Dada 2012) and is applicable for the adsorption of trace constituents. It was used by Ames et al. (1982) to describe adsorption of uranium and cesium onto basalt and its weathering products. Equation 1.7 can be linearized as:

$$\ln C_s = \ln C_m - K_D \epsilon^2 \quad (1.8)$$

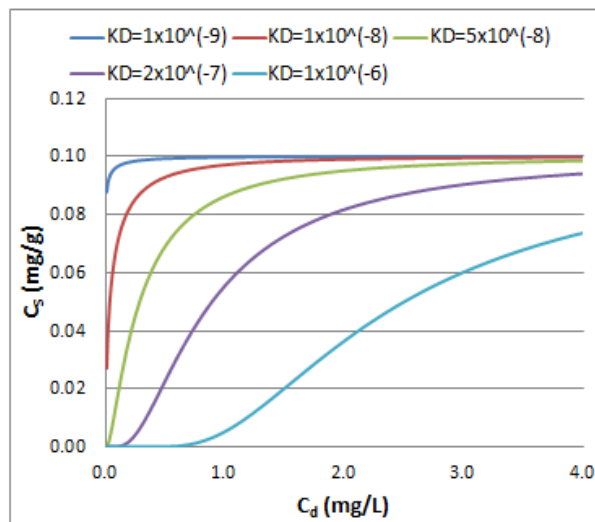
From the line that best fits the plot of $\ln C_s$ vs ϵ^2 , the value of C_m can be obtained from the intercept and K_D from the slope. The mean free energy (E_a) can be calculated from K_D using Equation 1.9, and its value indicates the main adsorption mechanism that is occurring ($E < 8$ denotes physical adsorption and $8 < E < 16$ implies ion exchange and $E > 16$ is associated to chemical adsorption) (Sun et al. 2022).

$$E_a = (2K_D)^{-0.5} \quad (1.9)$$

All three isotherm models can be compared with data from experiments that are performed by systematically varying the concentration of a contaminant or radionuclide while keeping all other parameters as constant as possible. It was stated by Giles et al. (1974) that isotherm shapes are largely determined by the predominant adsorption mechanism, and thus can be used to explain the nature of adsorption. The shape of the adsorption isotherm of each model varies according to the value of the parameters that define it, Figure 1.2 shows possible shapes that can be obtained from each model and serves as a reference to later identify which model can be fitted to the results obtained in this work.



(a) Langmuir model for $C_m = 0.1$ mg/g, K_L in L/mg. (b) Freundlich model for $K_F = 0.1$ mg/g.



(c) DR model for $C_m = 0.1$ mg/g, K_D in mol^2/kJ^2 .

Figure 1.2: Adsorption isotherm models shapes.

K_d determination

The most used methods to measure K_d values are (EPA 1999):

1. Batch in the laboratory
2. Batch in situ
3. Laboratory flow-through method (columns)
4. Modeling
5. K_{oc} method

Each method takes certain assumptions to determine the value of K_d from experimental

data, therefore, the most common and expected is that the values of K_d determined by different methods are different from each other. In this study, the method of batch experiments in the laboratory was used.

The batch method is the most commonly used to measure K_d in the laboratory, as the equipment, cost and time requirements are low and the methodology is simple. This method consists in adding a well characterized solid of known mass (M_{sol}) to a beaker with known volume (V_w) and concentration (C_0) of an aqueous contaminant solution. The beaker is then mixed until sorption is estimated to be complete (typically one to seven days). The resulting solution is centrifuged or filtered, and the remaining concentration of the contaminant (C_d) in the liquid phase is measured.

The concentration of adsorbate sorbed on the solid phase (C_s) is then calculated as:

$$C_s = \frac{V_w(C_0 - C_d)}{M_{sol}} \quad (1.10)$$

The value of C_d is measured directly in the laboratory, so the value of K_d (C_s/C_d) is:

$$K_d = \frac{V_w(C_0 - C_d)}{M_{sol}C_d} \quad (1.11)$$

One of the most common variations of the method is to perform a series of batch experiments that are identical except for the variation in the concentration of the dissolved contaminant, C_0 . Thus, the resulting K_d isotherm can be plotted from the corresponding data of C_d and C_s .

1.3 State of the art

The transport of contaminants from the phosphogypsum stacks to the Huelva estuary has been studied in several works. Pérez-López et al. (2016) carried out an assessment of their environmental impact and demonstrated the high potential of contamination of the whole stack, including the two zones that were supposedly restored, by studying samples of edge outflows taken from the perimeter channels. The analyzed leachates had a pH of 1.9 and concentrations of 6100 mg/L of P, 1970 mg/L of S, 600 mg/L of F, 200 mg/L of NH_4^+ , 100 mg/L of Fe, 10–30 mg/L of Zn, As and U, and 1–10 mg/L for Cr, Cu and Cd. Through the use of geochemical tracers it was deduced that the origin for the leachates is estuarine and not by percolation of the ponded process water, suggesting a possible tidal-induced leaching of the waste pile in depth. The mobility of natural radionuclides contained in the PG stacks has also been studied, being U-isotopes ($^{238-234}\text{U}$) (70 %) and ^{210}Po (50 %) the most mobile radionuclides and showing the Th-isotopes the lowest mobility (mobile fraction < 5 %) (Pérez-Moreno et al. 2018). In this same study, very

high activity concentrations of ^{210}Po (5-70 Bq/kg) and U-isotopes (3-500 Bq/kg) were found in the leachates, while the Th-isotopes and ^{226}Ra ones were 2 order of magnitude lower (0.01-1 Bq/kg).

There are not many studies carried out on treatments for the removal of contaminants and neutralization of leachates from phosphogypsum piles (PGL). Millán-Becerro et al. (2019) studied an alkaline treatment system for the PGL of Huelva by adding a $\text{Ca}(\text{OH})_2$ solution with the aim to increase their pH and subsequently, to provoke the precipitation and immobilization of the dissolved contaminants. This treatment achieved a phosphates and fluorides removal of 100 % and 90 %, respectively. For metals, removal values close to 100 % were reached for Fe, Al, Cr, Cd, U and Zn, whereas it did not seem to be totally effective for other elements such as As (removal of 57–82 %) and Sb (4–36 %). Also, Millán-Becerro et al. (2021) performed PGL batch experiments with alkaline materials from industrial waste (biomass ash) and commercial reagents for different solid/liquid ratios, reaching removal percentages close to 100 % for F, Fe, Zn, Al, Cr, U, Cu and Cd for experiments with ashes, while As showed a more conservative behavior in solution, reaching elimination values of only around 9–13 %. Pérez-Moreno et al. (2022) also studied a treatment for the neutralization of PGL by using different alkaline chemical reagents on a laboratory scale. The results showed that neutralization using $\text{Ca}(\text{OH})_2$ is the best option for the removal of their contaminants by precipitation, obtaining a clean liquid that could be discharged into the environment without any environmental impact. The removal of the components was strongly associated with the solution pH, among other aspects, for example, high pH values were required to achieve a considerable reduction in As concentration (pH \approx 9).

The effect of the increase of pH by seawater mixing on the mobility of pollutants in PG leachates has also been studied (Guerrero et al. 2021 and Papaslioti et al. 2018a). When gradually increasing the pH of PGL by mixing it with seawater until pH=7, it was observed that some elements, such as Al, Fe, Cr, Zn, Cu, Pb and U significantly decrease their concentration with increasing pH by sorption and/or precipitation processes, while other elements (Mn, Co, Ni, As, Cd and Sb) behave conservatively with no participation in sorption processes.

A passive treatment for PGL was studied in Millán-Becerro et al. (2020). The methodology for this consisted of columns flow-through experiments, using a combination of a fine-grained alkaline reagent scattered in a non-reactive matrix to raise the pH of the leachate and decrease the solubility of dissolved contaminants. Different alkaline reagents were used, including two industrial wastes (biomass ash and fly ash) for which the evolution in pH and concentration of anions and cations as a function of the treated volume was studied. The highest effectiveness was reached with $\text{Ca}(\text{OH})_2$, as it caused the highest removal of net acidity and the total removal of dissolved pollutants, but an improvement

in the chemical water quality was obtained with all alkaline reagents.

Up to the date of this work, no studies have been found on treatments for the decontamination of PGL with red mud from the aluminum industry, but there have been several studies on the use of red mud for the treatment of other acid drainages, as well as adsorption studies with various metals. In the work of Bai et al. (2022), the treatment of heavy metal pollutants (Pb, Cu and Cd) in water by applying red mud particle waste was studied, analyzing the effect of reaction time, red mud dosage, temperature and pH on removal efficiency. Their experiments demonstrated that the amounts of this heavy metal ions removed increased with increasing red mud dosage and with pH. Also, the adsorption rate exceeded 90 % for the three elements when the solution pH was in the neutral range. Another research (Chen et al. 2022), focused on the removal of U from radioactive wastewater by various red mud particles with different size fractions (from >75 to $< 5 \mu\text{m}$), concluding that red mud with a size fraction of $< 5 \mu\text{m}$ exhibited the largest adsorption capacity and that the U adsorption by red mud was well described by the Langmuir model. In another study (Khaitan et al. 2009) the acid neutralization capacity of Jamaican red mud was measured by titration with HCl to pH endpoints of 4.5, 6, 8 and 10, which was found to be 1.8 and 0.5 mEq/g RM for titration to pH 4.5 and 10, respectively.

The use of red mud for arsenic (As) removal from water and the adsorption process that entails has been widely investigated. The study of White et al. (2003) showed that red mud efficiently removed As(III) in the pH range between 7.6 and 9.0 and As(V) in the pH range between 5.5 and 6.0, and that pre-washing the red mud with salt water improved its arsenic adsorption capabilities. The As adsorption isotherm was studied, and it was found that it properly fitted the Langmuir isotherm model.

Research has also been done on the use of red mud as an adsorbent for the removal of chrome (Cr) from aqueous solutions. For example, red mud activated with HCl was used for chromate removal by Dursun et al. (2008), where about 70 % chromate removal efficiency was obtained with the optimum red mud dose and pH.

The potential of nickel (Ni) removal from aqueous solution with red mud was analyzed in some works, such as Zouboulis and Kydros (2007). Red mud acted simultaneously as an alkalinity regulator, causing precipitation of Ni as the insoluble hydroxide, as an adsorbent of the formed nickel hydroxide and as a flocculant of the resultant fine particulate matter. Langmuir and Freundlich adsorption isotherms presented good fits with the experimental data.

Agrawal et al. (2004) investigated the adsorption behaviour of copper (Cu) on red mud, finding that the maximum adsorption of Cu was at pH 5.5 and that the Langmuir and Freundlich models did not fit well with the equilibrium data. Nadaroglu et al. (2010) also

examined the potential of red mud for Cu removal from water and the results showed that the adsorption of Cu increased with increasing pH, with maximum adsorption of Cu at initial solution pH of 5.5 as well.

This work intends to study the neutralization capacity of two red muds of different origin, as well as the mechanisms of adsorption and removal efficiency of various potentially toxic elements, particularly those present in high amounts in PGL. As high concentrations of multiple elements are present simultaneously, PGL is a particular effluent for which the behavior of contaminants with red mud has not been previously studied.

1.4 Objectives

The general objective set for this work is to characterize alkaline residues generated in the aluminium industry for their use in the decontamination of phosphogypsum leachates.

To meet this general objective, the following specific objectives are proposed:

1. To do a literature review on removal of radionuclides and heavy metals in PGL, active permeable barriers, partition coefficients, adsorption isotherm models and red mud characterization.
2. Sample the PG leachates and acquire the alkaline solid residues.
3. Perform a pretreatment and physicochemical characterization of solid wastes and PGL.
4. Determine the acid neutralization capacity of residues by means of titration curves with HNO_3 and H_3PO_4 .
5. Determine the optimal solid/liquid ratio for the treatment of PGL and identify the main acids present by means of titration curves.
6. Perform a physicochemical characterization of the liquids and solids obtained in the neutralization processes of the PGL to evaluate the ability of the residues to remove contaminants.
7. Carry out batch experiments and characterize the resulting liquids to study the K_d and the interaction between the most relevant contaminants present in the PGL and the alkaline residues.

2 Materials and methods

This section describes the sampling, materials, methods, and laboratory techniques used during this study.

2.1 Samples and materials

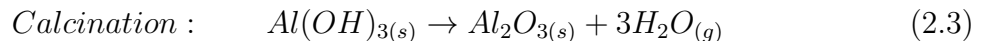
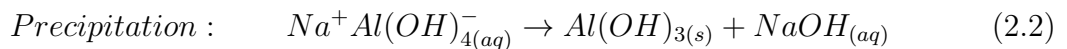
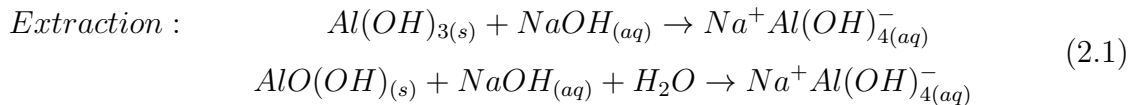
In February 2022, four samples of leachate were collected from the perimeter channels of the phosphogypsum stacks, two from zone 2 and two from zone 3. For this study the sample from zone 3 was used, called Z3 (1) and coded 22-1045-A.

Three industrial and one domestic ash waste materials were used, before describing each one specifically, the process from which the industrial waste comes will be briefly explained.

Bayer process for alumina production

This process is the main industrial method used to obtain alumina (aluminum oxide, Al_2O_3) from bauxite. Bauxite contains about 30–60 % aluminum, expressed as Al_2O_3 , the rest being a mixture of silica, various iron oxides, and titanium dioxide (McLachlan et al. 1998). Aluminium compounds are present as gibbsite ($\text{Al}(\text{OH})_3$), boehmite (AlOOH) and diaspore ($\alpha\text{-AlO}(\text{OH})$).

The process (Figure 2.1) consists of the digestion of crushed bauxite in concentrated sodium hydroxide solution in a pressure vessel at temperatures of up to 270 °C. At these temperatures, the aluminium compounds are dissolved as sodium aluminate (primarily $[\text{Al}(\text{OH})_4]^-$) in an extraction process (Equation 2.1), leaving an insoluble residue (red mud) which is removed by settling/filtration. After separation of the residue, gibbsite ($\text{Al}(\text{OH})_3$) is precipitated when the liquid is cooled and then seeded with fine-grained aluminum hydroxide crystals from previous extractions (Equation 2.2) (Hind et al. 1999). Finally, about 90 % of the gibbsite produced is converted into Al_2O_3 , by heating in rotary kilns or fluid flash calciners to a temperature of about 1200-1300 °C (Equation 2.3). The main reactions that take place during the process are then:



The vast majority of the obtained alumina is later used for the production of aluminium metal by electrolysis. The waste product that is generated in the digestion of bauxite with sodium hydroxide is called red mud, a highly alkaline slurry (pH 10–12.5) (Zouboulis and Kydros 1993). When dried it forms a fine powder composed primarily of silica (3-50 %), aluminium (10-20 %), iron (30-60 %), calcium (2-8 %), sodium (2-10 %) and titanium (0-25 %) oxides and hydroxides (along with other minor components), red in color due to the iron impurities (Khairul et al. 2019). Its chemical composition is very complex and depends largely on the characteristics of the bauxite source. Due to its high calcium and sodium hydroxide content, it is relatively toxic and is an important potential source of pollution (Hind et al. 1999). A usual way of reusing part of this residue is through the production of ceramics. However, in this case the red mud will be used as reagent for PGL treatment due to its high alkalinity content.

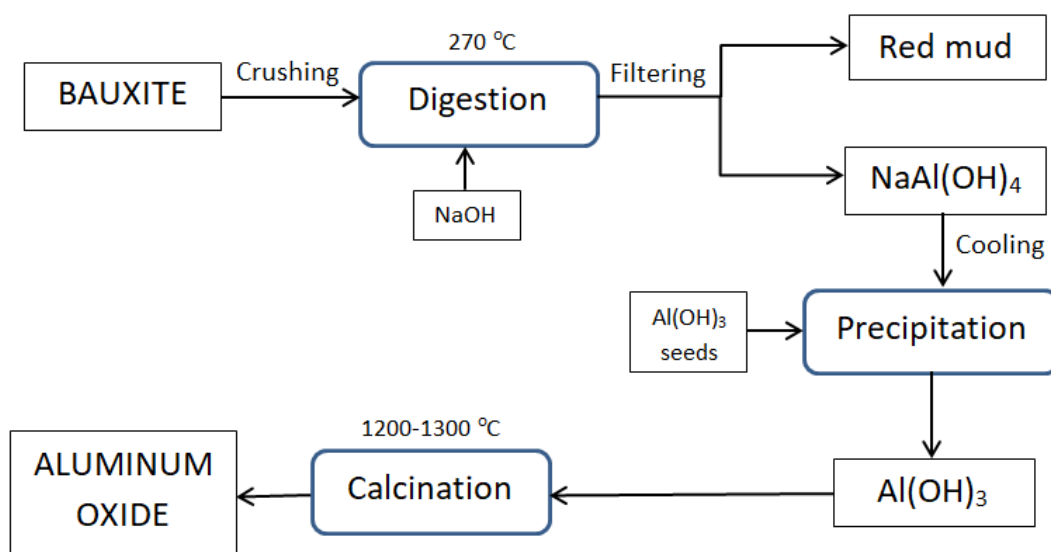


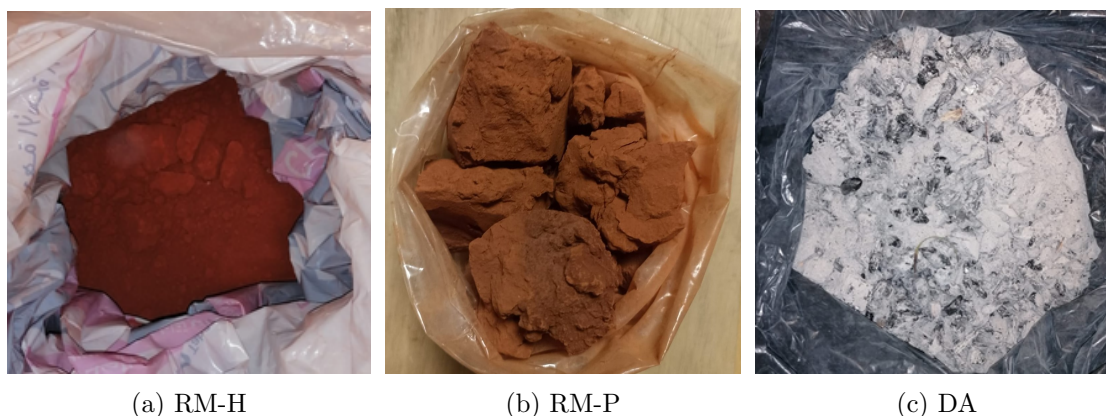
Figure 2.1: Scheme of the bayer process for alumina production.

Two red muds from different industries were used as alkaline waste in this study (Figure 2.2, Table 2.1):

- Red mud (22-1111, RM-P): waste generated during alumina production by the Bayer process. This residue came from Portugal through a collaboration with University of Aveiro but was originated in an industry of Spain.
- Red mud (21-1319, RM-H): waste generated during alumina production by the Bayer process. This residue is studied in the University of Huelva, but was originated in an industry from Saudi Arabia.

It was also decided to add domestic ashes collected from a fireplace, produced from eucalyptus wood (Figure 2.2). This ash residue was selected for comparison, since the ashes

from biomass combustion are commonly used for the neutralization of acidic effluents (Heviánková et al. 2014, Qureshi et al. 2016, Bogush et al. 2020), and have also been studied in some works for its use in the treatment of PGL (Millán-Becerro et al. 2020, Millán-Becerro et al. 2021).



(a) RM-H

(b) RM-P

(c) DA

Figure 2.2: Solid waste materials studied.

Table 2.1: Waste materials used and their corresponding numerical and alphabetic codes.

Residue	Numerical code	Alphabetic code
Red Mud Huelva	21-1319	RM-H
Red Mud Portugal	22-1111	RM-P
Domestic Ash	22-1112	DA

Several solutions were prepared for the following experiments, such as NaOH 1.5 M, HNO₃ 1.1 M, HNO₃ 0.55 M, H₃PO₄ 0.5 M and HCl 2 M.

2.2 Pre-treatment

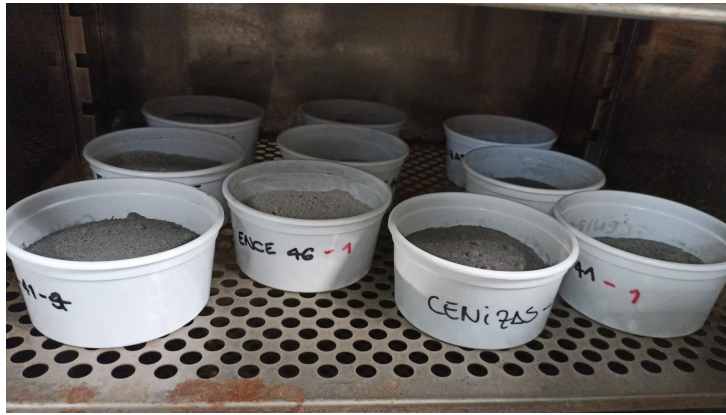
Drying: Approximately 1 kg of each solid waste were taken and dried at 60 °C in plastic containers until their mass was constant from one day to the next (Figure 2.3a).

Grinding: Both RM-P and RM-H were ground so that their sifting was possible, since they were originally agglomerated in lumps larger than 63 microns and only a very small portion passed through this sieve. A vibratory disc mill (Retsch RS 100) was used, grinding each sample for 5 minutes at 700 rpm (Figure 2.3b).

Sieving: All the dried and grinded samples were sieved in three fractions: F1 (< 63 μm); F2 (63 μm < x < 500 μm); F3 (> 500 μm). The ashes passed easily through the sieve,

while RM-H and RM-P formed a film on the 63 μm sieve that did not allow the rest of the sample to pass through, and the sieving had to be done manually with the help of a brush. The time in the sieving machine was between 5 and 20 minutes depending on the sample, 5 minutes for the ashes and up to 20 minutes for both the RM before manual sieving (Figure 2.3c).

Digestion: An acid digestion was performed to all of the solid samples to prepare them for ICP-MS and ICP-OES analysis. About 0.5 g of the smaller than 63 μm fraction from each solid sample were digested using 9 mL HNO_3 , 2 mL HCl , 3 mL HF and 2 mL H_2O_2 . The sample mixtures were then heated at 100 $^\circ\text{C}$ for 24 hours in a closed vessel. The samples were then cooled and transferred to a teflon vessel washing the previous one with 5 mL of HCl . This was evaporated to dryness, then 6 mL of HClO_4 were added and evaporated to dryness again. Finally, 10 mL of HNO_3 were added and evaporated to dryness two times. The final solids were diluted in a HNO_3 2% solution to a volume of 50 mL.



(a) Drying



(b) Grinding



(c) Sieving

Figure 2.3: Solid residues pre-treatment.

2.3 Analytical techniques

2.3.1 Alpha spectrometry

Alpha spectrometry is a technique that aims to determine of the energy distribution of the alpha particles emitted by a radioelement, and in this way, determine of the activity concentration of a specific radionuclide in a sample (Bq/kg , Bq/m^3).

Alpha particles produce a high total ionization but have little penetration into matter (because of their large size), they are absorbed in a few microns of solid matter. To minimize the absorption of alpha particles in the sample before reaching the detector (self-

absorption), the sample must be deposited on a very thin film. Additionally, detection is performed in a vacuum chamber to minimize absorption of alpha particles by the air.

In this case a Passivated Implanted Planar Silicon (PIPS) detector was used. The procedure to which the sample is subjected prior to its placement in the detector, both for the isolation of each radioelement and the deposition on the thin film, is included in the radiochemical method which consists of the following steps:

- Sample collection and pretreatment
- Addition of tracer
- Pretreatment (concentration for liquid samples or digestion for solid samples)
- Chemical isolation by tributylphosphate (TBP) and purification with ionic resin
- Deposition onto counting disc
- Count in an alpha spectrometer
- Calculation of tracer recovery and sample activity

The added tracer consists of an artificial radioisotope, which behaves chemically the same as the studied radionuclide but has different alpha emission energy, and the objective of its addition is to determine the total recovery of the process.

In this study, the PGL and the liquid phases from all batch experiments were analysed by alpha spectrometry and the samples were not pre-treated. Also, only the radionuclide ^{210}Po was analyzed, because the radioelements U and Th were detected by ICP-MS. The tracer used was ^{209}Po (105.6 ± 0.2 mBq/mL).

Since Polonium is not extracted with the organic solvent, the separation step for the other radioelements was not performed and Po was directly isolated by self-deposition on a silver disc, which was finally analyzed in the alpha spectrometer to later calculate the activity concentration.

The activity concentration is calculated according to the methodology implemented by the FRYMA research group (Blasco et al. 2016).

The alpha spectrometry was performed using an EGG Ortec system with an integrated Octete PC PLUS with eight chambers. Each chamber consists of a 450 mm² ion-implanted silicon PIPS detector, each one housed inside a vacuum chamber. In addition, each alpha spectrometer chamber includes a vacuum gauge, variable detector bias supply, a preamplifier, a shaping amplifier with adjustable gain, a pulse stretcher, and bias amplifier, a test pulse generator with variable amplitude, and a leakage current monitor. The detectors have a maximum FWHM (Full Width Half Maximum) of 20 keV and a detection efficiency close to 25 % for distances less than 10 mm. A background counting rate of

fewer than 30 counts per day is expected in the energy range from 3-8 MeV. The detectors operate at a polarization voltage of 50 V. The program used to control individually the spectrometer and for spectrum analysis and data, evaluation was Maestro.

2.3.2 Inductively coupled plasma optical emission spectrometry (ICP-OES)

ICP-OES is a technique used to identify and quantify the elements present in a sample using two components: an ionization source (ICP) and a spectrometer (OES).

The sample is generally introduced in liquid form, and undergoes several processes on entering the ICP: a nebulizer is used to transform the sample to aerosol, which then enters a spray chamber that allows only suitable sized droplets to pass through to the plasma. After entering the plasma, the sample is desolvated, vaporized, atomized and ionized by the high temperatures that are reached (6000 to 10000 K).

The torch consists of three concentric tubes wrapped at one end by a radiofrequency coil. The atomized sample enters through the central tube, the plasma gas (Ar) through the next tube, and a cooling gas on the outside. Through the coil a magnetic field of great intensity is generated at the outlet of the torch, a spark is applied to the gas generating argon ions which are captured by the magnetic field and originate a chain reaction of ionization that ends in the transformation of gas in plasma (Thomas 2001).

When these ionized or excited atoms in the plasma recombine or return to their base state, they emit electromagnetic radiation, whose wavelength is characteristic of each element. In addition, the amount of radiation emitted is proportional to the analyte concentration, which makes the quantification of each element possible by comparing it with previously measured patterns.

Mirrors and lenses direct the light emitted by the atoms and ions in the plasma into the spectrometer. Inside the spectrometer, the light is separated, so the intensity of the light can be measured at different wavelengths by the detector.

The samples were analyzed by ICP-OES in the laboratory CIC of Granada with Perkin-Elmer Optima 8300 ICP-OES Spectrometer and in CIDERTA laboratory of Huelva with Agilent 5110 VDV Spectrometer.

2.3.3 Inductively coupled plasma mass spectrometry (ICP-MS)

The ICP-MS technique uses the same ionization source (ICP) as ICP-OES, but in this case the ions are detected by a mass spectrometer (MS).

When leaving the ICP, the sample passes through an interface made up of two metallic cones with very small holes, which are kept under vacuum. Then, the ion lens transports the ions from the cone outlet to the mass analyzer and prevents particles, neutral species,

and photons from reaching the mass analyzer. The quadrupole mass analyzer is the most commonly used, it consists of four cylinders that, when applying certain voltages, only allow the passage of ions in a specific m/z range, which then produce an electric current that is measured by the detector and translated into a concentration.

ICP-MS is a fast, highly sensitive, multi-element technique with a wide dynamic range. It can detect most elements on the periodic table in concentrations up to ppt, making it particularly suitable for ultra-trace analysis of elements. Its spectra are relatively simple and it has a low level of interference.

The samples were analyzed by ICP-MS in the laboratory CIC of Granada, with NexION 300D Spectrometer and CIDERTA of Huelva with Agilent 7700/JP Spectrometer.

2.3.4 Ion Chromatography

Ion exchange chromatography is a technique that allows the separation of ions and polar molecules based on the electrical charge properties of the molecules.

The sample is carried by a buffered aqueous solution, known as the mobile phase, to the chromatography column which contains an analyte in stationary phase, or ion exchanger. The stationary phase carries fixed electrostatic charges on its surface, which have the function of retaining counterions from the mobile phase as it passes through the column. The target analytes are conserved in the stationary phase and can then be eluted by applying a pH gradient to the column with a buffer. Finally, the analytes of interest can be detected in various ways, typically by conductivity or absorption of UV or visible light.

The samples were analyzed using ion chromatograph 883 Basic C.I. plus, from Metrohm in CIDERTA laboratory from the University of Huelva.

2.3.5 X-Ray Fluorescence (XRF)

X-Ray fluorescence is used to identify atoms present in a sample and their abundances. This technique consists of a solid or a liquid sample being irradiated with high energy X-rays from an X-ray tube, when an atom in the sample is struck with an X-ray of sufficient energy, an electron from one of the atom's inner orbital shells is dislodged. The vacancy left in the inner orbital shell is filled with an electron from one of the atom's higher energy orbital shells to regain stability. When it drops to a lower energy orbital, the electron releases energy in the form of X-rays, along a spectrum of characteristic energies that allow to identify the atoms present in the sample. Depending on the intensity of the fluorescent X-rays emitted, it is possible to know the abundances of each element present in the sample.

1.5 g of the smaller than 63 μm fraction from each solid residue were analyzed by XRF.

Major elements were determined by X-ray Fluorescence sequential spectrophotometer PANanalytical (model ZETIUM Minerals) in the Central Research Services of the University of Seville (Spain), this equipment allows qualitative and quantitative chemical analysis from O to U in a wide range of concentrations from major to trace components.

2.3.6 X-Ray Diffraction (XRD)

X-ray diffraction (XRD) analysis is a technique used to determine the crystallographic structure of a material based on their diffraction pattern.

This technique consists of irradiating the sample with an X-ray beam, which is scattered by crystal atoms when hitting the material, primarily through interaction with the atoms' electrons. A regular array of scatterers produces a regular array of spherical waves, in most directions this scattered waves cancel each other out through destructive interference, however, they add constructively in a few specific directions, which are determined by Bragg's law. The intensities and scattering angles of the diffracted patterns are detected, and later interpreted, by comparison with standard reference patterns, to identify crystalline forms present in the sample.

To analyze the samples by XRD, approximately 2.2 g of each solid were mixed with 0.3 g (12% of the total mass) of zincite (ZnO) and ground in a mortar until the mixture was homogeneous, then the sample was sieved with a 200 μm sieve. The zincite was added as an internal standard for amorphous fraction quantification.

The mineralogical characterisation of the powder samples was performed in the Central Research Services of the University of Seville (Spain) using X-ray diffractometer Bruker (model D8 Advance A25).

The crystalline mineral phases were identified using "Difrac. EVA" software with PDF4/Mineral database, and the quantification of the phases was carried out according to the "Rietveld" method using the "Difrac. Topas" software.

2.3.7 Quality control

The quality control applied in the ICP-MS and ICP-OES measurement was carried out by measuring three blanks and two reference standards. The certified concentration of the used standard was of 1000 ± 3 ppm of Ag, Al, B, Ba, Bi, Ca, Cd, Co, Cr, Cu, Fe, Ga, In, K, Li, Mg, Mn, Na, Ni, Pb, Sr, Tl and Zn. From this standards, solutions with concentrations of 51.22 ± 0.15 ppm and 50.01 ± 0.16 ppb were prepared, which were analyzed by ICP-MS and ICP-OES.

The relative difference between the values of concentrations measured by ICP-MS and the standard values were between -23 and 8 % for the laboratory CIDERTA of Huelva, without

taking into account the result of Cr which was 49 %. For the laboratory CIC of Granada the results showed greater relative differences, between 0 % and -44 % without taking into account the result of Li which was -74 %, which indicates that the measurement errors were systematic as all the measurements were lower than the certified value.

For ICP-OES technique, the solution of 51.22 ± 0.15 ppm was used for validation, resulting in relative differences between -1 and -7 % for the laboratory CIDERTA of Huelva and between -10 and -44 % for the laboratory CIC of Granada. Both results show a systematic error that underestimates the analyzed concentrations, being the errors of the measurements in CIC laboratory considerably higher.

Regarding the measurement of the blanks, most of the elements were not detected, or the confidence interval of the detected value contained the value zero.

The quality of the results obtained by XRF was validated by means of a correlation between the concentrations measured by XRF vs ICP-OES for the three solids analyzed (Figure 2.4). The three data sets were fitted to linear functions for which the slopes, y-intercept and R^2 values are shown in Table 2.2. The three were considered good correlations that validate the results obtained with the XRF technique, as the slopes are in agreement with 1 and the intercepts with 0.

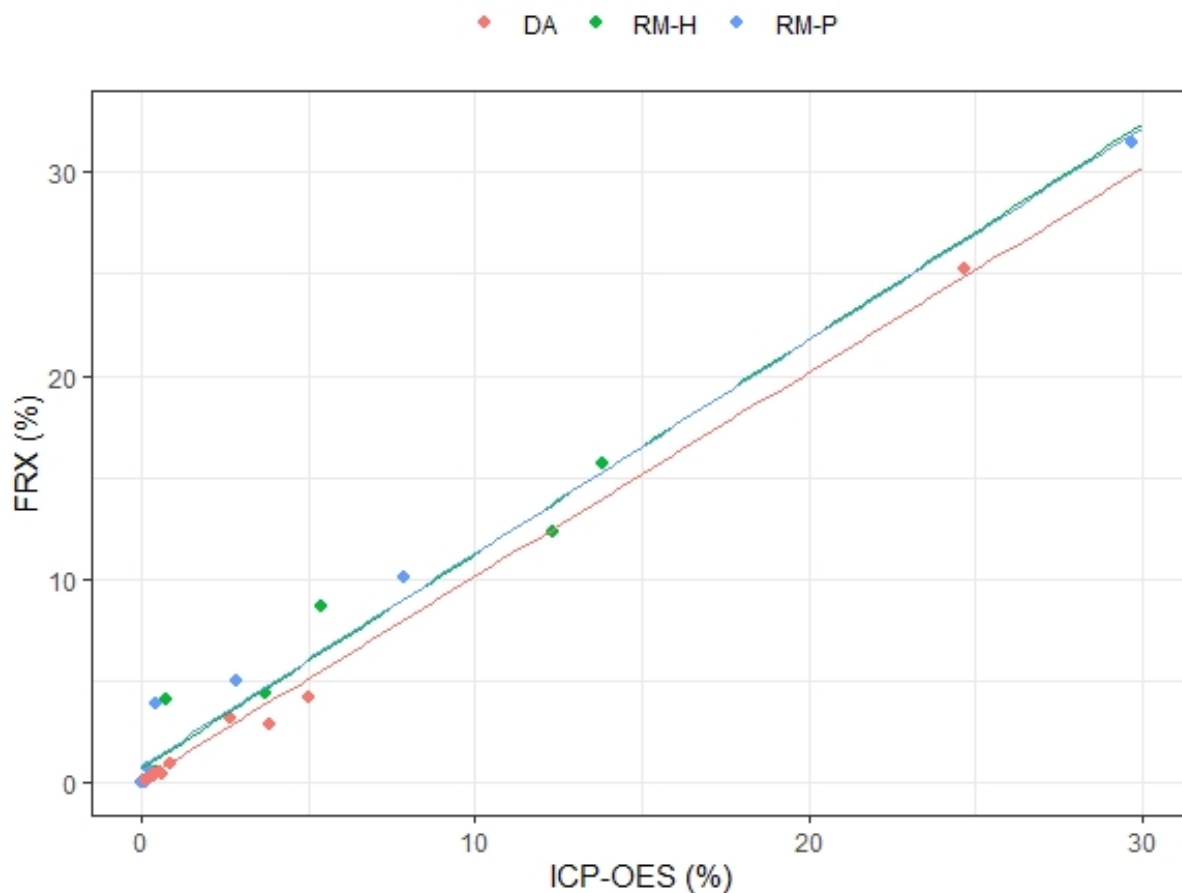


Figure 2.4: Comparison of major elements composition of the solids obtained by analysis of ICP-OES and XRF.

Table 2.2: Parameters and R^2 of the linear fits of XRF vs ICP-OES for the three studied solid wastes. Standard uncertainties are given.

	slope	y-interception	R^2
RM-H	1.05 ± 0.09	0.7 ± 0.6	0.944
RM-P	1.04 ± 0.05	0.9 ± 0.5	0.985
DA	1.02 ± 0.02	-0.15 ± 0.18	0.996

2.4 Design of experiments

2.4.1 Titration curves

This test consists of determining the Acid Neutralization Capacity (ANC) of the solid materials under study and identifying the acid species present in the PGL through titration

curves. These curves were performed both for PGL and for reference acids and bases. For all curves, the fraction of solid waste smaller than $63\ \mu\text{m}$ was used.

The titration curves experiments were carried out as follow. About 150 mL of acid dissolution (HNO_3 , H_3PO_4 and PGL) were taken, and a constant mass of alkaline material was added little by little (i.e in increments of 0.1 g or 0.5 mL) up to a stable pH. The solution was continuously stirred and the physicochemical parameters (time, pH, EC, ORP, temperature) were continuously measured (Figure 2.5). Finally, the solution was filtered with a $0.45\ \mu\text{m}$ pore filter, the resulting liquid was reserved for ICP-MS, ICP-OES, chromatography and alpha spectrometry analysis. The solid phase was dried until constant mass and reserved for analysis.

Experiment 1:

Objective: study the acid species present in the PGL.

- Reference dissolution: NaOH 1.5 M
- Acid dissolution: PGL

Experiment 2:

Objective: determine the ANC of different alkaline solid residues with HNO_3 .

- Reference dissolution: HNO_3 1.1 M and 0.55 M.
- Alkaline material: solid residues

Experiment 3:

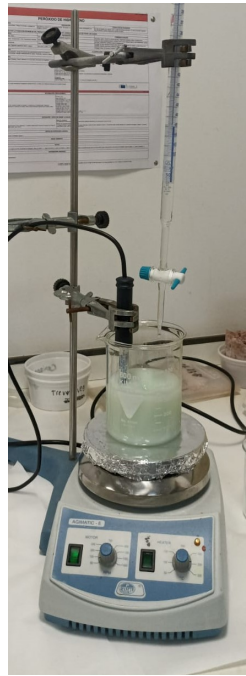
Objective: determine the behavior of different alkaline solid residues with pure H_3PO_4 to understand their behavior with the main acid present in the PGL.

- Reference dissolution: H_3PO_4 0.50 M
- Alkaline material: solid residues

Experiment 4:

Objective: determine the behavior of the alkaline solid residues as they neutralize the PGL, try to find their alkaline species and compare the results with the obtained titration curves by using pure H_3PO_4 .

- Reference dissolution: PGL
- Alkaline material: solid residues



(a) PGL with NaOH.

(b) Solid residues with HNO_3 , H_3PO_4 and PGL.

Figure 2.5: Experiment setup for titration curves.

2.4.2 Batch experiments

A series of batch experiments were carried out. The aim of this experiments was to study the interaction between each pollutant and the solid residues and to determine the partition coefficients (K_d) and adsorption isotherms.

For these experiments, the control of variables method was used. This consists of fixing all the variables except one, which is varied during each experiment.

Batch experiments consist of adding a well characterized granulated material of known mass into a beaker containing a known volume and concentration of an aqueous contaminant solution. The beaker is then mixed until sorption is estimated to be complete (24 h), or until the time determined for the experiment has passed. Different parameters such as solid/liquid ratio, initial concentration and contact time were evaluated in the batch

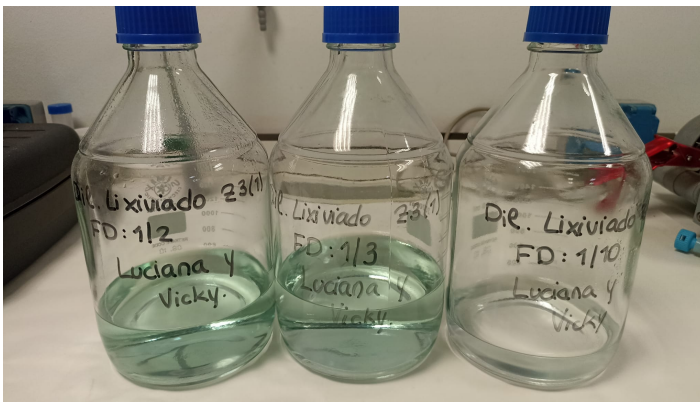
experiment.

The procedure for the experiments was to place about 150 mL of solution and the granulated waste (fraction smaller than $63 \mu\text{m}$) of known mass in vessels, with stirring (Figure 2.6). The solution was filtered after the corresponding contact time. Finally, the resulting liquid was reserved for ICP, ionic chromatography and alpha spectrometry analysis, and the physicochemical parameters (pH, EC, ORP, T) were measured. The solid phase was dried until constant mass and reserved for future analysis.

Four different batch experiments were performed (1A, 1B, 2A and 2B), whose variables are explained in table Table 2.3. The aim of the Batch experiments 1A and 1B was to determine the relation of K_d with the initial concentration of PGL (C_0). In this experiments, two different solid to liquid ratios (S/L) were used. The contaminant concentration that was adsorbed to the solid material after the experiments was calculated with Equation 1.10. Finally, the data was employed to study if the adsorption isotherms could be adjusted to any of the considered models. The aim of the Batch experiments 2 was to determine the variation of K_d and pH with contact time. In this experiments, two dilution factors (DF) and only one solid to liquid ratio were used.

Table 2.3: Variables of Batch experiments. Dissolution volume = 150 mL. Agitation = 230 rpm. S/L = solid to liquid mass ratio, DF = Dilution Factor ($C_0 = C_{0i} \cdot \text{DF}$, C_{0i} : original PGL concentration).

Experiment	S/L	DF	Contact time
1A	1/3.75	1/2, 1/3, 1/10, 1/30, 1/100,	24 hs
1B	1/7.50	1/250, 1/750, 1/2250	
2A	1/7.50	1/100	15 min, 30 min, 45 min, 60 min,
2B	1/7.50	1/10	250 min, 500 min, 1440 min



(a) PGL dilutions.



(b) Mixing of PGL dilutions with red mud.



(c) Solid and liquid separation by filtering after the experiment.

Figure 2.6: Batch experiments.

3 Results and discussion

3.1 PGL characterization

The PGL (22-1045) was characterized by ICP-MS, ICP-OES, ion chromatography and alpha spectrometry (Table 3.1) and its composition and physicochemical parameters were compared with the maximum values for emission allowed by regulations (Decreto 109/2015 2015) and background values for seawater (Guerrero et al. 2021, Papaslioti et al. 2018a, Nonose et al. 2014). As it is known, pH of PGL is very low, close to 1, and much lower than both the pH of seawater and the value allowed for discharges in coastal and transitional waters. The EC and Eh values measured slightly higher than the background.

The concentrations of all elements shown in Table 3.1 are higher than those found in seawater and those allowed for discharge. In particular the concentration of As, Cd, Cr, Cu, Fe, Mn, Ni, U and Zn is four to five orders of magnitude higher than the values of seawater; Al and Pb are also in very high concentrations, as they have values three orders of magnitude higher than seawater. The activity concentration of ^{210}Po , measured by alpha spectrometry is 117 Bq/L, well above the natural values in seawater (0.0036 Bq/L). The concentration of phosphates and fluorides in the PGL is also significantly higher than in seawater, more than 100 and 10 times respectively, as well as the sulphate content that is twice as high. This composition agrees with previous studies carried out on the PGL of Huelva (Pérez-Moreno et al. 2018, Papaslioti et al. 2018b, Pérez-López et al. 2016).

In relation to the limits established by the regulations, the element that exceeds them the most is Cd, exceeding the maximum allowed by three orders of magnitude, followed by Cr, Cu, Fe, Ni and Zn, which exceed it by two orders of magnitude. The concentration of fluorides and phosphates is also delimited by Decreto 109/2015 and is exceeded by the PGL by two and three orders of magnitude respectively.

These results reflect the high contaminant load of the PGL, of which a fraction is currently discharged into the Tinto estuary without any prior treatment, failing to comply with the limits established by Decreto 109/2015, which approves the regulation of discharges to the Hydraulic Public Domain and the Maritime-Terrestrial Public Domain of Andalusia.

3 RESULTS AND DISCUSSION

Table 3.1: Composition of PGL measured by ICP-OES, ICP-MS, ion chromatography and alpha spectrometry, background values and emission limits established by Decreto 109/2015 (2015).

Parameter	PGL	Background (Seawater)	Emission limit
pH	1.3	7.8	5.5-9.5
EC (mS/cm)	77	61	-
Eh (mV)	657	460	-
Element	mg/L	mg/L	mg/L
Al	264	0.13	10.0
As	96	<0.002	2.0
Ca	2140	440	-
Cd	20	<0.002	0.014
Cr	82	<0.002	0.36
Cu	26	0.004	0.90
Fe	197	0.008	3.6
Mg	3360	1440	-
Mn	56	<0.002	10.0
Ni	17	<0.002	0.72
Pb	2	0.003	0.26
Si	128	0.036	-
Ti	95		5.0
U	71	0.0032	-
Zn	129	0.050	1.8
Anions	mg/L	mg/L	mg/L
F ⁻	1160	111	17
Cl ⁻	28700	21700	-
Br ⁻	123	69	-
PO ₄ ⁻	102000	791	165
SO ₄ ⁻	7490	2740	-
Radionuclides	Bq/L	Bq/L	Bq/L
²¹⁰ Po	117	0.0036	-

Titration curve of PGL with NaOH

Titration is a technique to determine the concentration of an unknown solution. A solution of known concentration (titrant) is used to determine the concentration of an unknown solution (analyte). Typically, the titrant is added to a known volume of the analyte until the reaction is complete. Knowing the amount of titrant added allows to determine the concentration of the unknown analyte. In acid-base titrations, titrant and analyte is a pair of acid and base, this are monitored by the change of pH as titration progresses and the titration curve is the plot of the pH of the analyte solution versus the volume of the titrant added as the titration progresses.

From the titration curve, the equivalence point can be identified (Figure 3.1), this is the point at which the amount of titrant added is just enough to completely neutralize the analyte solution. At the equivalence point in a monoprotic acid-base titration, the number of equivalents of base are equal to the number of equivalents of acid. This point can be identified as the place on the curve where its concavity changes or its slope is the most vertical.

A midpoint, also shown in Figure 3.1 is when the number of equivalents of base added equals half of the number of equivalents of the monoprotic acid that are present, these can be identified on the titration curve from the buffer zone, a section with little or no pH variation. At the midpoint, pH equals the value of pKa because there is 50:50 mixture of the weak acid and the strong base, which makes it useful to identify the acidic species present in the analyte. To quantify this, the Henderson-Hasselbalch Approximation can be used (for a weak acid HA):

$$pH = pKa + \log \frac{[A^-]}{[HA]} \quad (3.1)$$

Since in the midpoint the concentrations of both A^- and HA are equal, $[A^-]/[HA]=1$, therefore: $pH=pKa+\log(1)$, so $pH=pKa$.

A polyprotic acid differs from a monoprotic acid because it has more than one H^+ , so it has the ability to donate multiple protons. When a weak polyprotic acid is titrated, there are multiple equivalence points because these will occur when an H^+ is dissociated (Figure 3.1). Therefore, the number of equivalence points depends on the number of H^+ atoms that can be removed from the molecule.

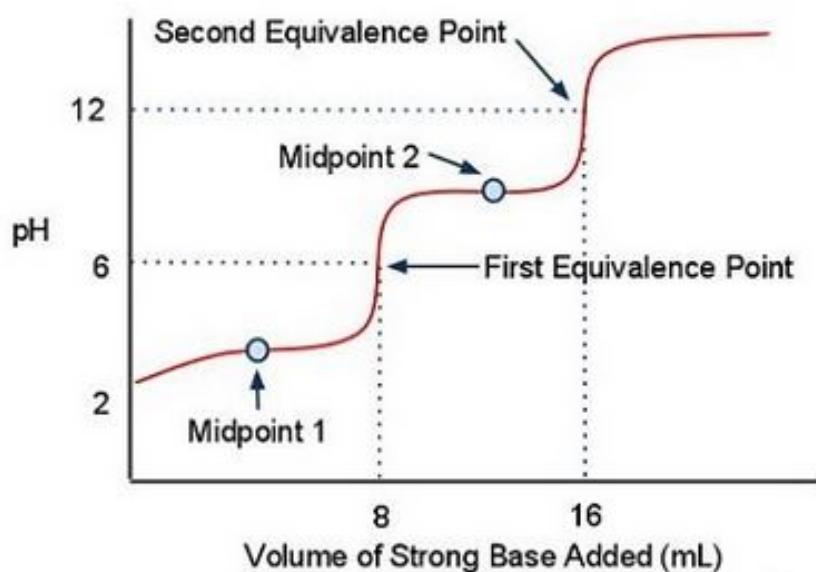


Figure 3.1: Scheme of a titration curve of a diprotic acid with a strong base. Extracted from *Titration of a Weak Polyprotic Acid*, 2022, LibreText Chemistry (<https://chem.libretexts.org>).

From the titration curves, information on which acids are present in the analyzed solution can be obtained by comparing the pK_a values obtained experimentally with the pK_a values of known acids.

A titration curve of PGL was made with NaOH 1.5 M, a strong base (Figure 3.2), with the aim of determining the acids present in the PGL from the analysis of the buffer zones of the curve and the comparison of their midpoints with the pK_a value of known acids. In this curve, three buffer zones were identified, their midpoints were obtained by taking the value of the half of the plateau on the abscissa axis and looking for the pH value of the corresponding point of the curve.

The experimentally obtained midpoints (designated as pK_e) indicated in Figure 3.2 correspond to: $pK_{e1}=1.8$, $pK_{e2}=6.1$ and $pK_{e3}=11.4$. These values of pK_a are very close to those found in phosphoric acid (H_3PO_4 : $pK_{a1}=2.2$; $pK_{a2}=7.2$, $pK_{a3}=12.7$). Therefore, it can be deduced that the main acid species present in the studied PGL is phosphoric acid ($H_3PO_4(aq)$), this acid is expected to be present in the PGL, since it is a product that is formed together with the PG in the industrial process and therefore it is predictable that there are remnants of it in the PG which are later leached. Another sub-product from phosphoric acid production that is expected to be present in the PGL is hydrofluoric acid ($HF(aq)$), which pK_a value is $pK_a = 3.2$ and is not clearly detected in the titration curve from Figure 3.2. This is because HF is found in less quantity in the studied sample of PGL than H_3PO_4 , as it was shown in the ion chromatography results (Table 3.1) concentrations of PO_4^- are almost 100 times higher than F^- , which masks the neutralization of hydrofluoric acid in the titration curve.

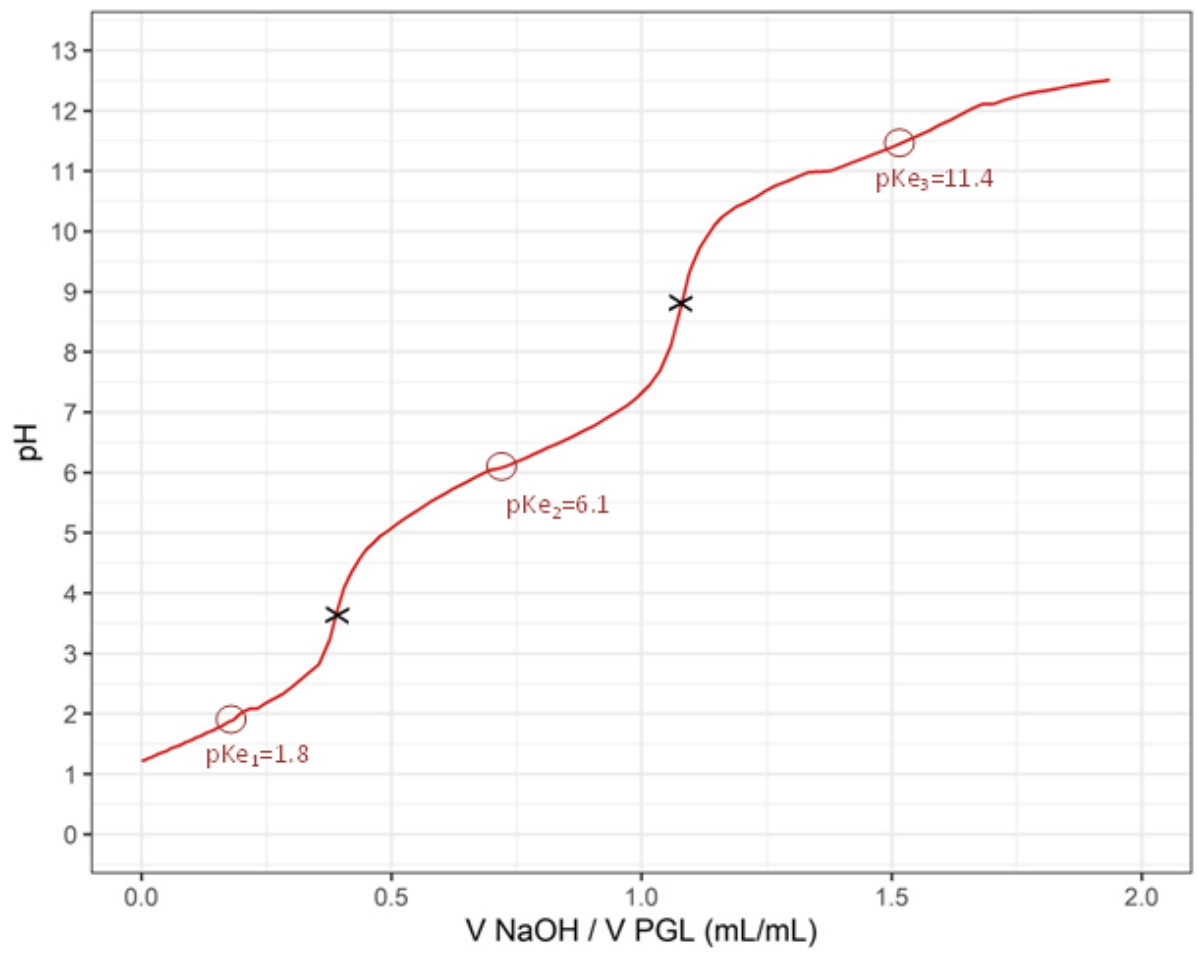


Figure 3.2: Titration curve of PGL with NaOH 1.5 M, circles symbolize midpoints and crosses equivalence points.

3.2 Solid waste characterization

All residues were measured for pH, electrical conductivity (EC) and Oxidation/Reduction Potential (Eh) (Table 3.2). All the residues have an alkaline pH (between 10.7 and 12.2), being the ashes (DA) slightly more alkaline than the muds (RM-H and RM-P).

Table 3.2: Solid waste characterization

Solid	pH	EC (mS/cm)	Eh (mV)
RM-H	10.7	14.0	216.4
RM-P	11.0	12.5	270.7
DA	12.2	21.7	116.0

Table 3.3 shows the particle size fractions resulting from the sieving of the solid waste materials. In the case of RM-P and RM-H these fractions are the ones resulting after grinding as they were aggregated in clods. For all the solids, a relatively high percentage of the fraction smaller than 63 microns was obtained. This fraction was the one used for all subsequent experiments, with the aim of maximizing the specific surface of the solid, and thus achieving a greater interaction between the residues and the PGL. The three sieved fractions are shown in Figure 3.3.

According to other studies (Khairul et al. 2019), red mud is typically a very fine-grained material. The particle size distribution is usually smaller than 75 μm for 90 wt% of red mud particles (Sutar et al. 2014), which coincides with the sieving percentage of both RM-H (82 % < 65 μm) and RM-P (86 % < 65 μm). Smořka-Danielowska and Jabłońska 2022 studied the grain distribution of various domestic ashes, finding that the fraction smaller than 100 μm is between 67 % and 84 %, which is compatible with the results obtained of the fraction smaller than 63 μm of 51 %.

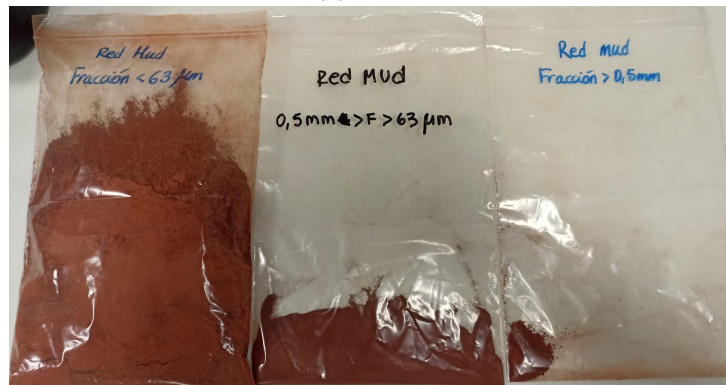
Table 3.3: Solid waste granulometry (%).

Solid	% > 0.5 mm	0.5 mm > % > 63 μm	% < 63 μm
RM-H	0.2	18	82
RM-P	0.4	14	86
DA	13	36	51

3 RESULTS AND DISCUSSION



(a) RM-H



(b) RM-P



(c) DA

Figure 3.3: Fractions of each solid residue obtained after sieving.

The fractions smaller than $63 \mu\text{m}$ of the solid residues were also characterized by ICP-MS, ICP-OES, X-ray fluorescence and X-ray diffraction.

The main elements in both red muds are Fe (16% to 32%) and Al (10% to 12%), followed by Na (5% to 9%) and Si (3% to 7%), RM-H also contains a 4% of Ca (Figure 3.4). Both residues come from the production of alumina from bauxite, which is a mixture of hydrated aluminium oxides and compounds of other elements such as iron. In the extraction phase of the process, bauxite is heated in a pressure vessel with sodium hydroxide solution

(NaOH), to convert it into soluble sodium aluminate ($\text{NaAl}(\text{OH})_4$). The red mud is the residue that is produced in this digestion, so it is expected to have a high content of iron oxides (which give them their characteristic red color), as well as aluminium oxides as process losses (Alkan et al. 2017, Khairul et al. 2019). The following main components of the red mud according to the studies of Alkan et al. (2017) and Khairul et al. (2019) are Si, Ti, Na and Ca oxides, which agrees with the results obtained by XRF and ICP-OES. The composition of the solids was also compared with typical soil values determined by Rudnick and Gao (2013) (Figure 3.4). Both red muds have an Al and Ca content similar to typical soil, while their Fe content is an order of magnitude higher. They also possess an order of magnitude less K, Mg, and S than soil.

According to Smółka-Danielowska and Jabłońska (2022), who studied the composition of ashes from domestic wood-fired furnaces for different woods, the main components were in all cases Ca followed by K and Si. With a lower order of magnitude, there were followed by Mg, P, Al and Fe. This is in agreement with the results for the domestic ashes of this study, composed mainly of Ca (25%), followed by K (4%) and Mg (4%). In smaller amounts they also contain Na, Si, P, S, Al and Fe. The ashes, unlike red mud, compared to a typical soil, have an Al and Fe content one order of magnitude lower (0.4 %) and one order higher content of Ca. Its content of K and Mg is similar to that of the soil. The three residues studied have a Na content similar to that of the typical soil (3 % to 9 %) and higher S (0.1 % to 0.6 %), Si (1 % to 7 %) and P (0.1 % to 1 %) values.

Potentially toxic elements, such as As, Be, Pb, Cd, Zn, Cu, Ni, Cr, Sb, Tl and Zn were present to some extent in all solids (Figure 3.5). Taking as a reference the values of generic reference levels (NGR) for trace elements in Andalusia defined by Decreto 18/2015, which establishes the legal regime applicable to contaminated soils, as well as potentially contaminated soils, none of the solids exceeded any of these established levels to determine if a soil is potentially contaminated.

Comparing the trace elements content of the solids with the typical soil, both red muds contain more Ag (41-46 times), As (2 times), Cd (3-6 times), Cr (6-16 times), Cu (2-5 times), Hg (6 times for RM-H), Pb (4-5 times), Th (6-10 times) and U (3-5 times), having RM-H higher concentration than RM-P of most trace elements, while the rest of the elements are found in similar or lower concentrations. The DA have a significantly higher content of Ag (22 times), As (5 times), Cu (9 times), Pb (4 times) and Zn (6 times) than typical soil.

3 RESULTS AND DISCUSSION

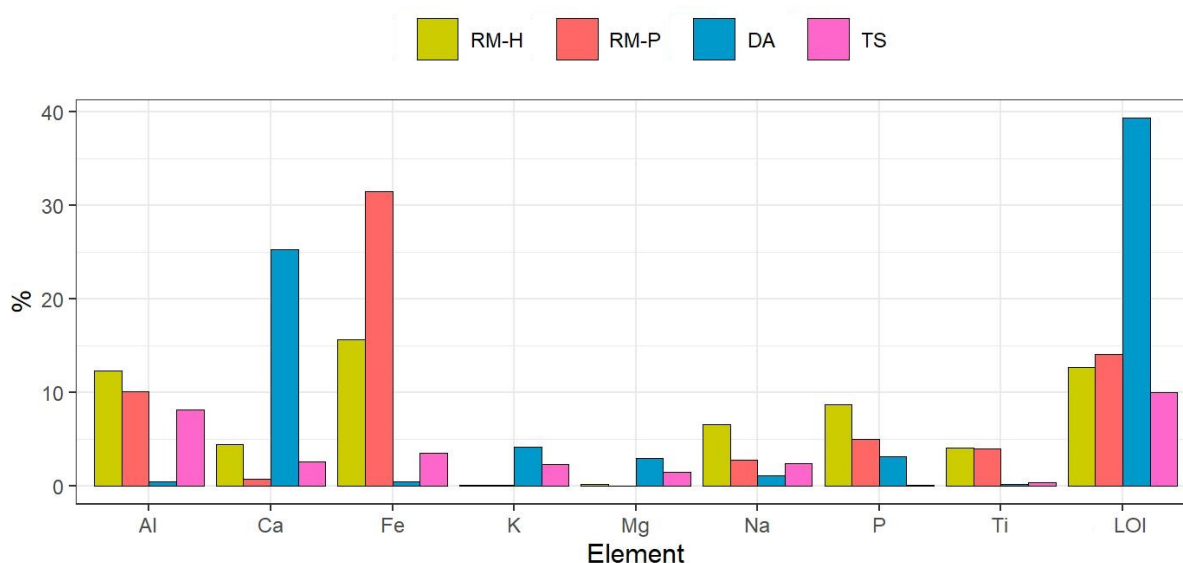


Figure 3.4: Solid waste mayor elements and typical soil (TS) composition values. LOI: loss on ignition.

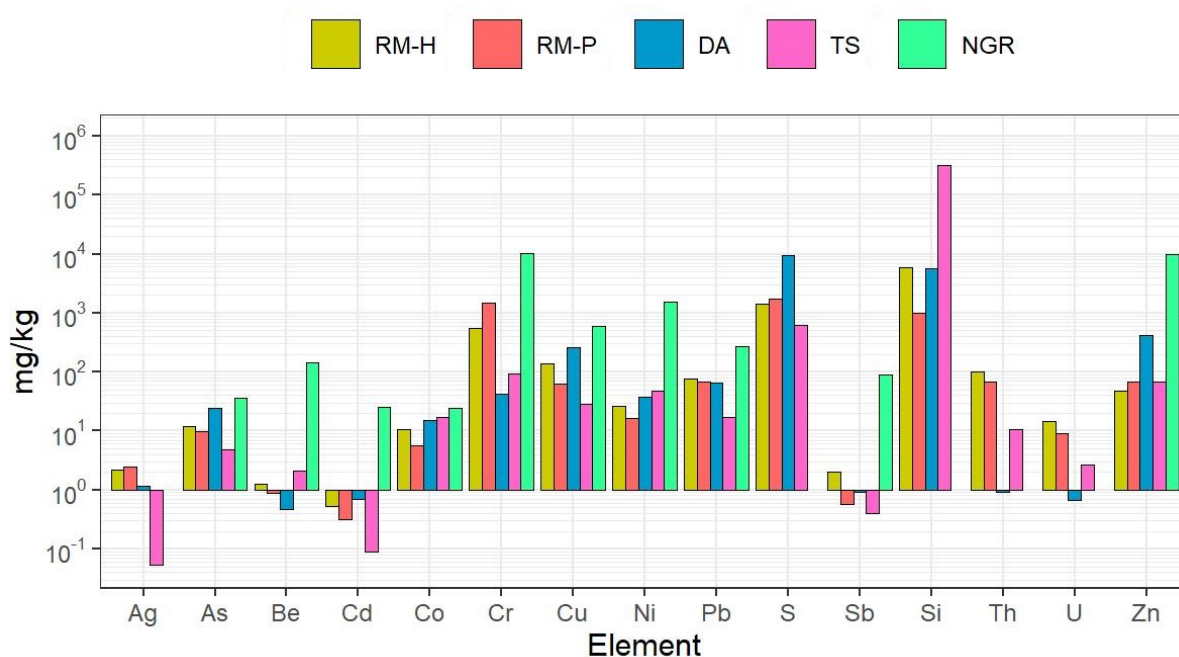


Figure 3.5: Solid waste trace elements composition, NGR and typical soil (TS) composition values.

Mineral phases present in the solids were identified by XRD. The crystalline phases are shown in the diffraction patterns of Figure 3.6 and their proportions as well as the amorphous fractions are indicated in Table 3.4. For the three solids, at least one third of their composition was found to be amorphous (32 % in RM-H, 42 % in RM-P and 33 % in DA).

The main mineral phases contained in RM-H are 13.8 ± 0.6 % of cancrinite ($\text{Na}_6\text{Ca}_2\text{Al}_6\text{Si}_6\text{O}_{24}(\text{CO}_3)_2$), 12.3 ± 0.5 % of hematite (Fe_2O_3), 7.8 ± 0.6 % of rutile (TiO_2), 7.0 ± 0.9 % of ilmenite (FeTiO_3) and 6.5 ± 0.5 % of sodalite ($\text{Na}_{7.88}(\text{Al}_6\text{Si}_6\text{O}_{24})(\text{CO}_3)_{0.93}$). In this solid, it was also found a 4.1 ± 0.3 % of calcite (CaCO_3), 3.9 ± 0.3 % of boehmite ($\text{AlO}(\text{OH})$), 3.5 ± 0.4 % of goethite ($\text{FeO}(\text{OH})$) and 2.9 ± 0.4 % of gibbsite ($\text{Al}(\text{OH})_3$). In RM-P the main mineral phases identified were 21.3 ± 0.6 of hematite (Fe_2O_3), 18.6 ± 1.2 of iron oxide hydroxide ($\text{FeO}(\text{OH})$) and 7.5 ± 0.6 of gibbsite ($\text{Al}(\text{OH})_3$).

Various studies (Gräfe et al. 2011, Samal et al. 2013, Liu and Naidu 2014) have reported the presence of all this mineral phases in red mud from multiple countries of origin.

These mineral phases present in the red mud can be explained by two origins: the phases that are originally present in bauxite and are transferred to the red mud such as boehmite, gibbsite, hematite, goethite, rutile and anatase. On the other hand, there are phases formed during the alkali digestion, such as sodium aluminum hydrosilicates, titanates of sodium, calcium, or magnesium and calcined aluminum silicate (Srikanth et al. 2005). During the Bayer process, several chemical additives can be added, such as lime ($\text{Ca}(\text{OH})_2$), iron oxides (Anon 1967), MgSO_4 (Pohland and Schepers 1985) or apatite, to aid processes such as flocculation and separation. This Ca inputs, explain the presence of Ca minerals that are formed and remain in the residue, such as calcite and cancrinite.

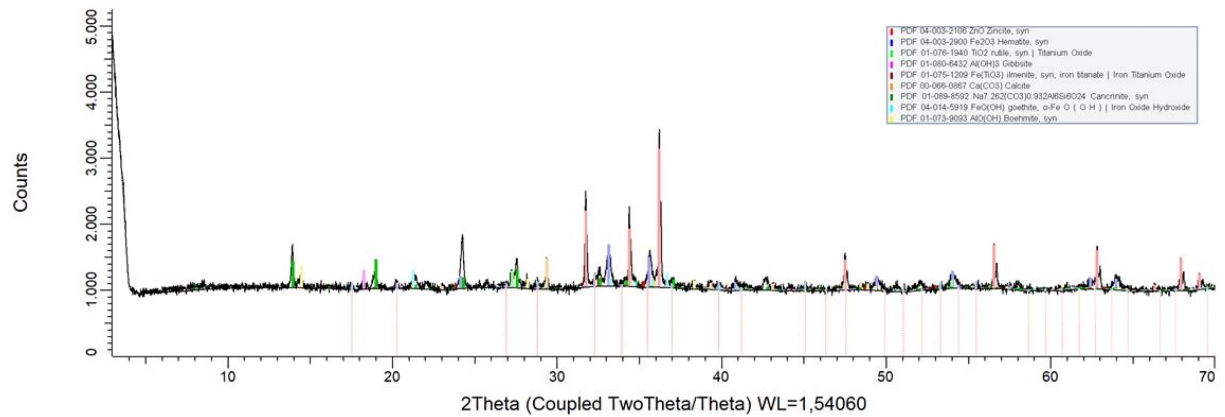
The DA contains mainly calcium carbonate (CaCO_3 : 49.1 ± 0.6 %) and in less amount halite (NaCl : 4.89 ± 0.19 %), periclase (MgO : 4.1 ± 0.3 %), silvite (KCl : 3.54 ± 0.10 %), quartz (SiO_2 : 1.02 ± 0.09 %) and lime ($\text{Ca}(\text{OH})_2$: 0.85 ± 0.09 %). The presence of these minerals agrees with the high values of Ca, followed by smaller amounts of K, Na, Mg and Si detected by XRF (Figure 3.4).

The mineralogical composition of ash from wood combustion was determined in various studies (Vassilev et al. 2013, Maresca et al. 2017) in which all of the phases previously mentioned were found to some extent. The study of Smółka-Danielowska and Jabłońska (2022) determined that the dominant components measured in domestic ashes with a size smaller than $100\ \mu\text{m}$ by XRD were calcite (CaCO_3), fairchildite ($\text{K}_2\text{Ca}(\text{CO}_3)_2$), periclase (MgO), monetite (CaHPO_4), and quartz (SiO_2), in different proportion depending on the type of wood burnt.

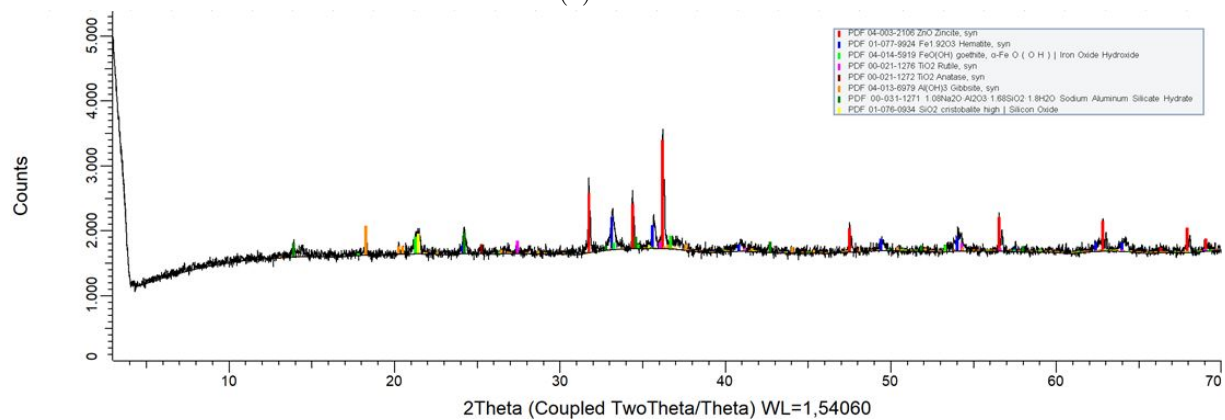
Quartz is expected to be found in ash from wood biomass as it is a common soil component (Sano et al. 2013). Periclase and silvite may represent a residue of Mg and K incorporated into the organic matter (Koukouzas et al. 2009), as they are typical plant nutrients. According to Canti (2003), ash that forms from plant matter burning contain calcium carbonate as a main component, coming from the calcium present in the cellular minerals (carbonates or oxalates) and the cell walls which end up recrystallised as carbonate once the ash has absorbed enough moisture and CO_2 from the air after burning.

3 RESULTS AND DISCUSSION

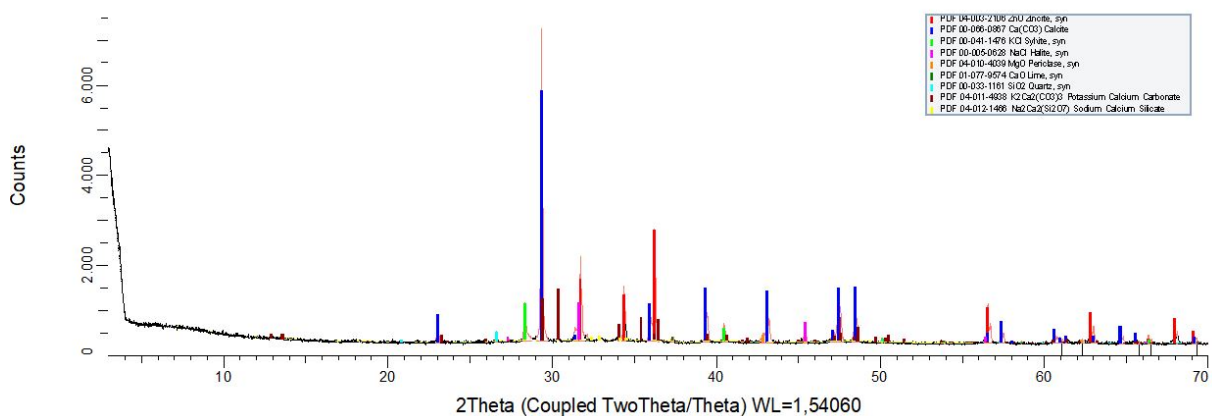
To evaluate the quality of the fit achieved with the Rietveld method used for the characterisation of the crystalline materials, the following indices were considered: GoF (goodness of fit), Rp (profile residual), Rwp (weighted profile residual) and R-Bragg (Bragg residual). Values of $GoF < 1.2$, $Rp < 3$, $Rwp < 4$, $R-Bragg \leq 2$ were obtained for red muds and $GoF < 1.5$, $Rp < 6$, $Rwp < 8$, $R-Bragg \leq 8$ for DA. These values are considered as indicators of a good fit between the calculated and experimental pattern.



(a) RM-H



(b) RM-P



(c) DA

Figure 3.6: Diffraction patterns of the solid wastes.

3 RESULTS AND DISCUSSION

Table 3.4: Mineral and amorphous phases identified and quantified in the solids by XRD in %.

RM-H		RM-P		DA	
Amorphous	38.1±1.7	Amorphous	48.4 ±1.7	Amorphous	36.5 ± 0.8
Cancrinite (Na ₆ Ca ₂ Al ₆ Si ₆ O ₂₄ (CO ₃) ₂)	13.8±0.6	Hematite (Fe ₂ O ₃)	21.3±0.6	Calcium Carbonate (CaCO ₃)	49.1 ± 0.6
Hematite (Fe ₂ O ₃)	12.3±0.5	Iron Oxide Hydroxide (FeO(OH))	18.6±1.2	Halite (NaCl)	4.89 ± 0.19
Rutile (TiO ₂)	7.8±0.6	Gibbsite (Al(OH) ₃)	7.5±0.6	Periclase (MgO)	4.1 ± 0.3
Ilmenite (FeTiO ₃)	7.0±0.9	Silicon Oxide (SiO ₂)	2.2±0.5	Silvite (KCl)	3.54 ± 0.10
Sodalite (Na _{7.88} (Al ₆ Si ₆ O ₂₄)(CO ₃) _{0.93})	6.5±0.5	Rutile (TiO ₂)	1.3±0.3	Quartz (SiO ₂)	1.02 ± 0.09
Calcite (CaCO ₃)	4.1±0.3	Anatase (TiO ₂)	0.8±0.3	Lime (Ca(OH) ₂)	0.85 ± 0.09
Boehmite (AlO(OH))	3.9±0.3				
Goethite (FeO(OH))	3.5±0.4				
Gibbsite (Al(OH) ₃)	2.9±0.4				

3.3 Study of the acid neutralization capacity of solids

3.3.1 Titration curves

In this section, the results of titration curve experiments of the three residues studied are discussed, first with a strong acid (HNO_3), then with a weak acid, H_3PO_4 , which is the main acid present in PGL, and finally with the leachate under study (PGL).

The main objective of these experiments was to know the acid neutralization capacity of the alkaline residues, that is, how much solid is necessary to add to neutralize each solution, what is the maximum pH that can be reached, in addition to defining the amount of solid to be used in the batch experiments with PGL.

Titration curves of HNO_3 with residues

Figure 3.7 shows the results of the variation of pH of a HNO_3 solution when adding each solid residue. For DA a solution of HNO_3 1.1 M was used. For RM-H and RM-P, a solution of HNO_3 0.55 M was used instead, because too large an amount of solid was needed to achieve the increase in pH with the 1.1 M solution.

Nitric acid in aqueous solution completely dissociates, so it has no pKa and the plateaus that occur in its titration curve are indicative of the characteristics of the added solid. That is, the hydroxides present in the solid dissolve when in solution and consume protons, producing an increase in pH in the solution as the solid is added.

In both the RM-H and RM-P curve (Figure 3.7) three buffer zones are observed. The first one at pH close to 0.5, the second one at approximately pH = 3.2 and another near pH = 7 for RM-H and 8 for RM-P, where the pH finally stabilizes and stops increasing. The buffer zones that occur at pH 3.2 are probably caused by precipitation of iron hydroxides, which occurs at pH \approx 3.5 (Xu and Gao 2008). The Fe^{3+} in solution comes from the iron compounds present in the red mud added up to that point that were dissolved due to the low pH. In the DA curve, two plateaus occur, the first one at the beginning of the curve close to pH = 0 and the second when the pH stabilizes and stops increasing at pH \approx 9.

The acid neutralization capacity (ANC) of an alkaline waste is a measure for the overall buffering capacity against the change in pH (Wahlström et al. 2013) and it is quantitatively defined as the number of acid equivalents that is capable of neutralizing. Different minerals can neutralize acid drainage at different rates and in different pH ranges (Lawrence and Scheske 1997). From these titration curves with nitric acid, an estimate of the total ANC with respect to pH=7 was determined for each solid, following the estimation method used in Khaitan et al. (2009), as molar mili Equivalents of HNO_3 per gram of residue (Table 3.6).

The equivalent in an acid–base reaction is the amount of a substance needed to react with

or supply one mole of hydrogen ions (H^+). In this way, the number of molar equivalents can be represented as the number of moles, multiplied by the number of protons (if it is an acid) or hydroxyls (if it is a base) that it releases. One equivalent of an acid reacts with one equivalent of a base. Therefore, the capacity of each residue to neutralize HNO_3 can be quantified as the ratio between the amount of acid equivalents used in the titration and the mass of residue needed to neutralize those equivalents (reach $pH=7$).

Of the three residues studied, the one with the highest HNO_3 neutralization capacity was DA (16 mEq/g residue), followed by RM-H and RM-P which had very similar ANC of 2.0 and 1.8 mEq/g respectively (Table 3.6).

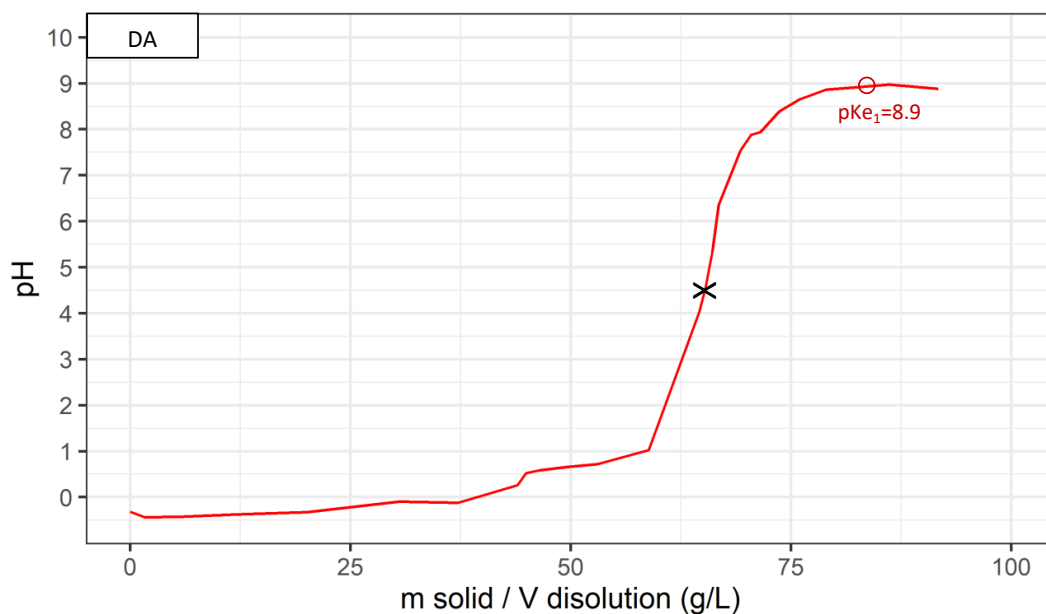
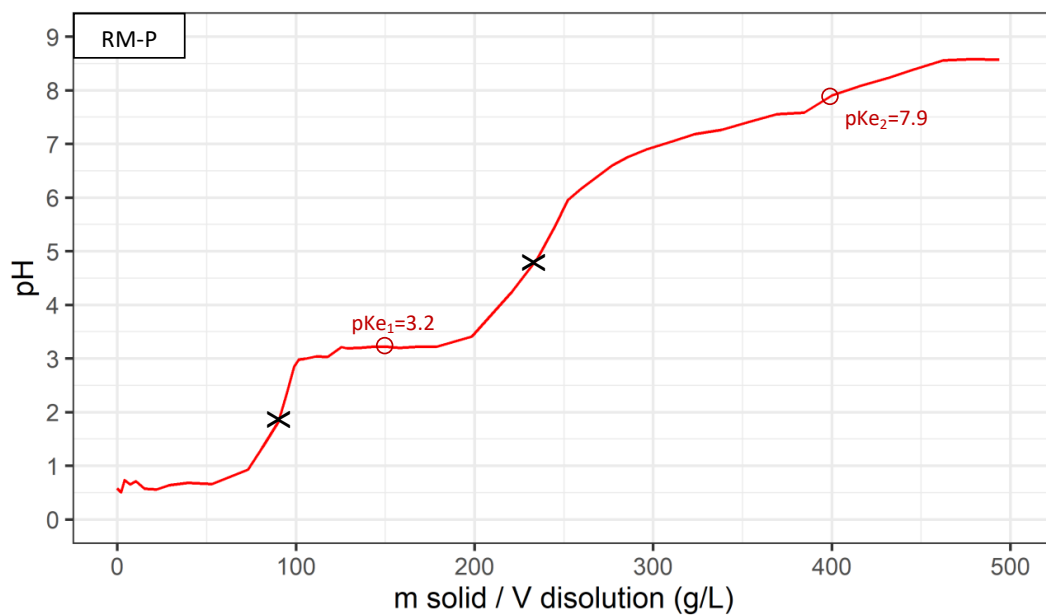
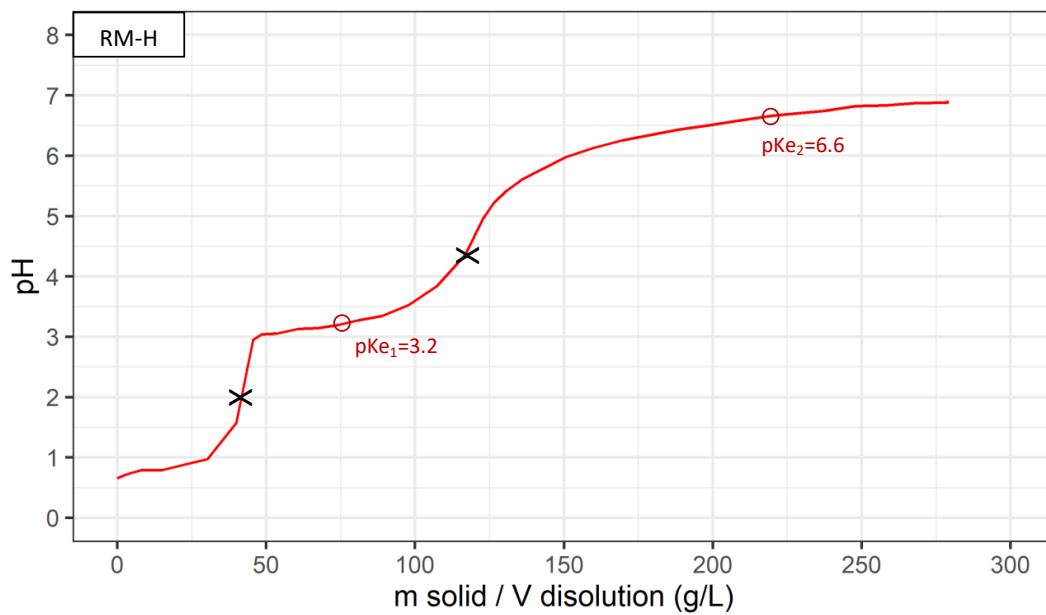


Figure 3.7: Titration curves for RM-H, RM-P and DA with HNO_3 0.55 M (RM-H and RM-P) 1.1 M (DA). Circles represent midpoints and crosses equivalence points.

Titration curves of H_3PO_4 with residues

The titration curves of a 0.5 M H_3PO_4 solution with each residue are shown in Figure 3.8 alongside the titration curves of PGL for ease of comparison. This acid was selected since it is the main one that is expected to be found in the PGL. Unlike the neutralization curve of HNO_3 , when a weak acid is titrated with a weak base (moreover, in this case the solid is composed of a mixture of bases), the pH plot does not show steep slopes, there is just a “point of inflexion” at the equivalence point, where the slope slightly changes, which was considered for the determination of the midpoints indicated in the figure.

In the RM-H curve, two plateaus are observed, which, considering their midpoint, are identified with the values of $\text{pKe}_1 \approx 2.6$ and $\text{pKe}_2 \approx 7.0$. According to bibliography (García-García et al. 2020, Gouider et al. 2009), both coincide approximately with the first two dissociation values of H_3PO_4 ($\text{pKa}_1 = 2.2$, $\text{pKa}_2 = 7.2$).

In the RM-P curve, two similar buffer zones are observed, which are identified with the midpoint values of $\text{pKe}_1 \approx 2.2$ and $\text{pKe}_2 \approx 7.5$, which also coincide approximately with the pKa_1 and pKa_2 values of H_3PO_4 ($\text{pKa}_1 = 2.2$, $\text{pKa}_2 = 7.2$).

In the DA curve, three more pronounced plateaus are produced, one at $\text{pH} \approx 3.2$, the next at 5.4 and finally at 7.9 where the pH stabilizes and stops increasing. The last buffer zone could be associated to the second pKa of H_3PO_4 , but the first one is not clearly visible and pKe_1 and pKe_2 are produced by some of the hydroxides that form part of the solid.

The titration curves of H_3PO_4 with both red muds shows a very similar form with similar buffer zones, this is due to the fact that their composition is almost the same, unlike DA whose curve presents plateaus at different pH values and neutralizes the phosphoric with much less amount of solid. The most efficient solid for the neutralization of phosphoric acid was DA with a S/L ratio of 0.09, followed by RM-P and RM-H with S/L ratio 0.3 (Table 3.5), but in this case, higher final pH values were reached.

3 RESULTS AND DISCUSSION

Table 3.5: Comparison of results of HNO₃, H₃PO₄ and PGL titration curves with the different solids. $m_{dissolution} = 150$ g, S/L = Solid to liquid ratio for final pH.

	HNO ₃		H ₃ PO ₄		PGL	
	S/L	Reached pH	S/L	Reached pH	S/L	Reached pH
RM-H	0.28	6.9	0.29	7.0	0.43	6.8
RM-P	0.49	8.6	0.28	7.5	0.54	7.3
DA	0.11	9.0	0.09	7.9	0.22	7.3

As for HNO₃, the neutralization capacity of each residue with H₃PO₄ was calculated (Table 3.6), it is again observed that DA is the one with the highest ANC and RM-P has a similar ANC with H₃PO₄ as RM-H.

Table 3.6: Solid wastes acid neutralization capacity (ANC) of a strong and a weak acid in molar mili Equivalents / g of residue for pH=7.

	ANC(HNO ₃) (mEq/g)	ANC(H ₃ PO ₄) (mEq/g)	ANC(PGL) (mEq/g)
RM-H	2.0	4.3	3.1
RM-P	1.8	5.8	2.9
DA	16	17	8.7

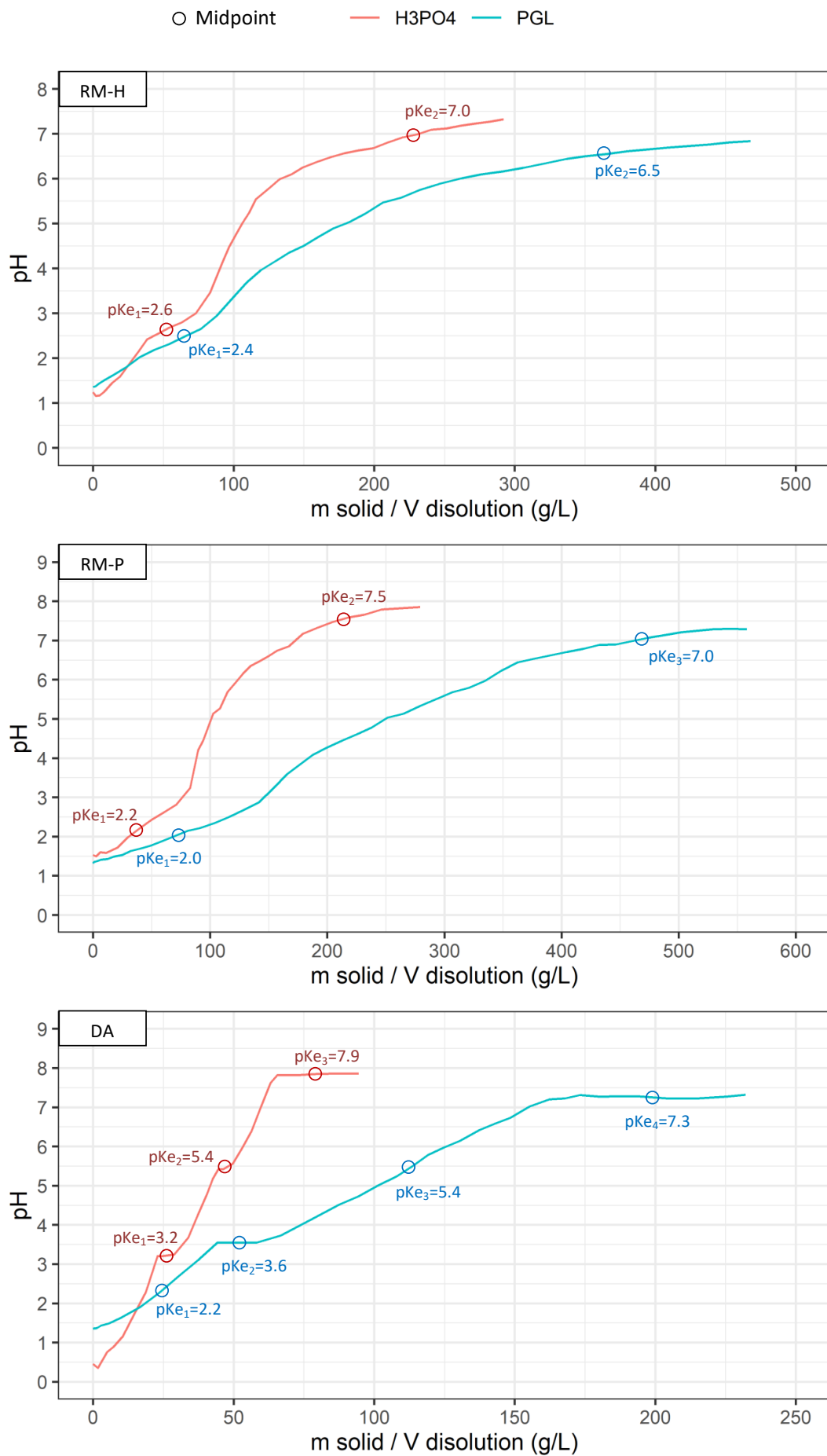


Figure 3.8: Titration curves for RM-H, RM-P and DA with H₃PO₄ 0.5 M and PGL.

Titration curves of PGL with residues

Next, the neutralization of PGL with each solid residue was studied. This titration curves were carried out to determine the necessary amounts of alkaline residue that must be added to achieve an increase in the pH of the PGL until a certain value. Figure 3.8 shows the results of the variation of the PGL pH when adding each solid residue.

Various buffer zones (in this case, as with H_3PO_4 , defined as parts of the titration curve in which the slope changes and remains constant for a certain section) were identified in the PGL titration curves, depending on the solid used.

For RM-H, two buffer zones were identified, the first one at the experimental midpoint (pKe) $\text{pKe}_1 \approx 2.4$ and the second one at $\text{pKe}_2 \approx 6.5$. These values could correspond to the first ones found in phosphoric acid (H_3PO_4 : $\text{pKa}_1=2.2$; $\text{pKa}_2=7.2$, $\text{pKa}_3=12.7$).

The RM-P curve has a similar shape to RM-H, two buffer zones were also identified: $\text{pKe}_1 \approx 2.0$ and $\text{pKe}_3 \approx 7.0$, which can also be identified with the $\text{pKa}_1=2.2$ and $\text{pKa}_2=7.2$ of phosphoric acid.

For the ashes (DA) four buffer zones were produced at $\text{pKe}_1 \approx 2.2$, $\text{pKe}_2 \approx 3.6$, $\text{pKe}_3 \approx 5.4$ and $\text{pKe}_4 \approx 7.3$. Three of these values could correspond to the values of pKa found in fluorhydric acid (HF: $\text{pKa}=3.2$) and to the first and second pKa of phosphoric acid (H_3PO_4 : $\text{pKa}_1=2.2$; $\text{pKa}_2=7.2$).

The acids identified in the PGL are the expected ones, since they are the products that are formed together with the PG in the industrial process and therefore it is predictable that there are remnants of them in the PGL.

Table 3.5 shows the maximum pH values reached for each residue, in which this measure stabilizes and stops increasing with the addition of solid. A maximum pH between 6.5 and 7.3 was achieved with all of them. This means that all the solids were able to neutralize the PGL and therefore are suitable for use in the treatment of PGL with an active or passive method, as PRBs, since the pH range allowed for discharge to the estuary is between 5.5 and 9.5.

The most efficient residue for PGL neutralization was DA, which required a solid/liquid ratio of 0.22. Double the solid/liquid ratio was needed for the neutralization of RM-H

(0.43), and the least efficient residue was RM-P, with which a solid/liquid ratio of 0.54 was needed.

For the three solids studied, the curves with PGL and H_3PO_4 have similarities in their shape and the pH values where buffer zones are produced, with the difference that more solid is required to increase the pH of the solution in the case of PGL, approximately double the solid/liquid ratio is needed in all cases to neutralize it, and slopes of buffer zones are more pronounced in the titrations with H_3PO_4 . This behavior can indicate that H_3PO_4 is the main acid present in PGL, but, unlike H_3PO_4 , the PGL contains a very high concentration of a variety of ions in solution, this can make the dissolution and interaction of solids with PGL less effective than with the dissolution of H_3PO_4 0.5 M. The ANC of both red muds with PGL was close to 3 mEq/g, less than with H_3PO_4 , for the same reason that the solid/liquid ratio is lower. ANC of DA with PGL is also higher (9 mEq/g) than ANC of red muds, the same way it happens with the other acids.

3.3.2 Removal of contaminants in titration curves

Once the titration curves of PGL with the solid residues were completed, the liquids resulting from the neutralizations were analyzed. In this section, the concentrations of various elements present the liquid phases are presented, with the aim of studying the removal capacity of different contaminants from each solid.

After the titration curve, the concentration of several of the elements in the PGL drops below the limit established by the regulations, in Table 3.7 the final concentrations are shown and those that remained above the limit (Decreto 109/2015 2015) are highlighted in red.

Table 3.7 also shows the effectiveness of each solid to treat the contaminants present in the PGL, considering that the volume of PGL is constant, assessed through the removal efficiency (RE %) of contaminants by each solid as:

$$RE(\%) = \frac{C_i - C_f}{C_i} \times 100 \quad (3.2)$$

where:

- C_i is the initial concentration of the element in the PGL (mg/L)
- C_f is the concentration of the element in the liquid phase filtered after the titration curve of PGL with each solid (mg/L)

The RE that did not achieve a value higher than 90 % are highlighted in blue in Table 3.7. The uncertainty of the RE was estimated considering the relative uncertainties of the measures of ICP-MS and ICP-OES $\sigma_r(C_i) = \sigma_r(C_f) = 5\%$, as:

$$\begin{aligned}\sigma_{RE}^2 &= \left(\frac{\partial RE}{\partial C_i}\right)^2 \sigma_{C_i}^2 + \left(\frac{\partial RE}{\partial C_f}\right)^2 \sigma_{C_f}^2 \\ \sigma_{RE} &= \left(\left(\frac{C_f}{C_i^2}\right)^2 \sigma_{C_i}^2 + \left(\frac{1}{C_i}\right)^2 \sigma_{C_f}^2\right)^{1/2}\end{aligned}\tag{3.3}$$

For non-conservative elements $C_i \gg C_f$, so the first term can be neglected and $\sigma_{RE} \approx \sigma_{r(C_i)} \approx 5\%$. For conservative elements $C_i \sim C_f$, so $\sigma_{RE} \approx \sqrt{2}\sigma_{r(C_i)} \approx 7\%$. Taking the least favorable value, $\sigma_{RE} = 7\%$ is considered.

The concentration of several elements (Al, Fe, Mn, Pb and Zn) was reduced below the established limit value with all the solids studied.

In the case of red muds, a high removal, close to 100 %, was also achieved for several elements that, although not limited by the regulations, were found in high concentrations in the PGL, such as: Ca, Co, Mg and U.

For other elements, although a high removal efficiency was achieved (between 75 and 100 %), this was not enough for the final concentration of the effluent to comply with the established limits, this was the case of Cd and Cr, being the final concentrations achieved 0.02 mg/L (RM-H) and 0.016 mg/L (RM-P) for Cd and 5.7 mg/L (RM-H) and 20.4 mg/L (RM-P) for Cr, surpassing the limits of 0.014 and 0.4 mg/L respectively.

For the experiment with RM-H, the best remotion of Cu was achieved, reducing its concentration from 26 mg/L to 0.16 mg/L, unlike RM-P that manages to reduce it to 5.9 mg/L. The same happens for Ni and Ti, which the RM-H manages to reduce from 17 mg/L to 0.23 mg/L and 95 mg/L to 0.044 mg/L respectively.

In the case of As, neither of the two red muds achieved a satisfactory removal efficiency

(52 % and 55 %), with the final concentrations obtained being 46 mg/L and 43 mg/L for RM-H and RM-P, respectively.

In general, higher removal efficiencies were achieved by RM-H compared to RM-P, even though the final pH reached was slightly lower (6.8 for RM-H and 7.3 for RM-P). All the elements studied suffer a removal above 90 % in the treatment with RM-H, with the exception of As, which only reaches 52 % and Si which reaches 68 %. With RM-P instead, several elements fail to be removed above 90 %, such as: As, Cr, Cu, Ni, P, Si and Ti.

The treatment of PGL with DA achieves satisfactory results in the removal of Al, As, Fe, Mn, Ni, P, Pb, Ti and Zn. The only contaminants that fail to reach a concentration accepted by the regulations are Cd, Cr and Cu, despite this, the reduction compared to the initial concentration is quite high: from 20 mg/L to 0.07 mg/L (100 %) for Cd, from 82 mg/L to 1.7 mg/L for Cr (98 %) and from 26 mg/L to 7.3 mg/L for Cu (72 %).

A clear difference can be seen in the behavior between the ashes and the red mud, for example in the case of Mg. In the curves with red mud, its concentration was reduced by 99 %, while with DA, RE only reaches 72 %, what can be explained because unlike for the red mud, the amount of Mg in DA is two orders of magnitude higher than in the PGL. Something similar happens with Ca and Cu, which do not achieve a high removal with DA, because the content of these elements in the initial solid is high, compared to the RM (1-2 orders of magnitude). On the other hand, As and P, despite being in higher concentration in the solid DA than in both RM, react much more favorably with the former, achieving nearly 100 % removal, while with the red muds, the final concentrations remain well above the discharge limit.

For the rest of the trace elements, large reductions in concentration were observed, the ashes being more effective in the case of Ti, Cr and As than the RM-P which only managed to reduce them by 76, 75 and 55 % respectively. Cu is the element for which the lowest reduction was achieved with DA, (72 %), and a similar value of 78 % was achieved with RM-P. Finally, very high reductions, close to 100% in Mn, Ni, Zn, Cd, Pb and U occurred for all solids, except for Ni with RM-P which was 89 %. The general higher removal efficiency of DA is in agreement with the work of Apak et al. (1998) who studied red muds and fly ashes as sorbents for heavy metal removal, finding the adsorption capacities

3 RESULTS AND DISCUSSION

of red muds were lower than those of ashes for the removal of the same metal ions.

Table 3.7: Initial concentration, emission limit established by Decreto 109/2015 2015, final concentration, and removal efficiency of studied elements in PGL titration curves with solids. Red indicates values above emission limit, blue indicates RE < 90 %.

Element	PGL	Limit	Final concentration			Removal efficiency ($\pm 7\%$)		
			PGL+RM-H	PGL+RM-P	PGL+DA	PGL+RM-H	PGL+RM-P	PGL+DA
	mg/L	mg/L	mg/L	mg/L	mg/L	%	%	%
Al	264	10.0	1.00	0.73	0.05	100	100	100
As	96	2.0	46.2	42.9	1.5	52	55	98
Ca	2137	-	24.1	0.31	174.8	99	100	92
Cd	20	0.014	0.02	0.016	0.07	100	100	100
Co	2.09	-	0.018	0.0088	0.0080	99	100	100
Cr	82	0.4	5.7	20.4	1.7	93	75	98
Cu	26	0.9	0.16	5.9	7.3	99	78	72
Fe	197	3.6	1.00	0.09	0.04	99	100	100
Mg	3364	-	38.4	30	1535	99	99	54
Mn	56	10.0	0.021	0.033	0.06	100	100	100
Ni	17	0.7	0.23	1.8	0.27	99	89	98
P	23810	60.0	1904	3231	7.8	92	86	100
Pb	2	0.3	0.010	0.018	0.00	100	99	100
Si	128	-	41	17	31	68	87	76
Th	0.093	-	0.0077	0.028	0.0027	92	70	97
Ti	95	5.0	0.044	23.0	0.27	100	76	100
U	71	-	0.0084	0.080	0.94	100	100	99
Zn	129	1.8	0.077	0.38	0.11	100	100	100

In summary, the solid residue that seems to be more effective for the removal of contaminants up to a permitted level is DA, since it only fails for three elements (Cd, Cr and Cu), followed by RM-H, with which in this test (under these specific conditions) only As, Cd, Cr and P do not reach acceptable values of final concentration. The least efficient solid was RM-P, which fails to efficiently remove seven contaminants: As, Cd, Cr, Cu, Ni, P and Ti. The red muds were selected as residues to study the partition coefficient, since a different ash with similar behavior to DA is already being studied in another work. In the following section, the results of the batch experiments carried out with the objective of studying the partition coefficient of the RM-H and RM-P with the contaminants under

different conditions are analyzed.

3.4 Batch Experiments

This section shows the results obtained for Batch experiments 1 (varying the PGL dilution factor) and 2 (varying the contact time) both performed with the residues RM-H and RM-P. The objective of these experiments was to study the interaction mechanisms between the contaminants present in the PGL and the alkaline solids. More specifically to study the variation of the partition coefficient under different conditions. A good understanding of this solid-contaminant interaction is necessary so that in the future a PGL treatment can be designed using permeable reactive barriers that adequately retain the target contaminants. From the analysis of the adsorption isotherm model which best adapts to the experimental data, the most probable interaction between the particulate material and the PGL or other liquid under treatment can be estimated.

3.4.1 Batch experiment 1

Based on the results of the PGL titration curves, and since the most concentrated dilution to be used has a dilution factor of 1/2, it was decided to perform the first batch experiments with 40 g and 20 g of solid, which is half the amount needed to neutralize 150 mL of PGL with the least efficient red mud (RM-P). This results in a solid/liquid ratio (S/L) of 1/3.75 for experiment 1A and 1/7.5 for experiment 1B.

In experiments 1A the variable under study was the dilution factor (DF), and the constant conditions were:

- Solid mass = 40 g
- PGL dilution mass = 150 g
- Contact time = 24 h

As expected, the pH results show that the more diluted the PGL is, the higher the pH it reaches after 24 h, for the same amount of solid (Table 3.8 and Figure 3.9). The values increase rapidly in the less diluted experiments and appear to have an asymptotic trend towards a pH close to 10.5. For this first S/L, the pH reached by the different PGL dilutions is practically the same for both red muds.

3 RESULTS AND DISCUSSION

In experiments 1B the variable under study was also the dilution factor, and the constant conditions were:

- Solid mass = 20 g
- PGL dilution mass = 150 g
- Contact time = 24 h

The pH variation of this experiment occurs in the same way as for 1A (higher final pH the greater the dilution), with the difference that the pH values are lower, since less alkaline solid was added, until the last three dilutions where the final pH is almost the same for both experiments, slightly higher than 10. In this second experiment, with a lower S/L, a difference is observed in the final pH values for the two residues, but only in the first two dilutions (1/2 and 1/3) where, with RM-H, higher values are reached, with differences of 2.0 and 1.4, while for the rest of the dilutions the final pH values are very similar for the two red muds.

Table 3.8: pH results of Batch experiments 1A (S/L = 1/3.75) and 1B (S/L = 1/7.50).

Dilution	Initial pH	Final pH			
		1A RM-H	1A RM-P	1B RM-H	1B RM-P
1/2	1.6	7.2	6.8	6.2	4.8
1/3	1.7	7.5	7.3	7.0	5.6
1/10	2.0	8.6	8.7	7.7	7.9
1/30	2.2	9.3	9.7	8.8	9.0
1/100	2.5	9.8	10.3	9.2	10.0
1/250	2.7	10.1	10.6	9.9	10.3
1/750	3.0	10.3	10.5	10.3	10.5
1/2250	3.4	10.4	10.6	10.2	10.4

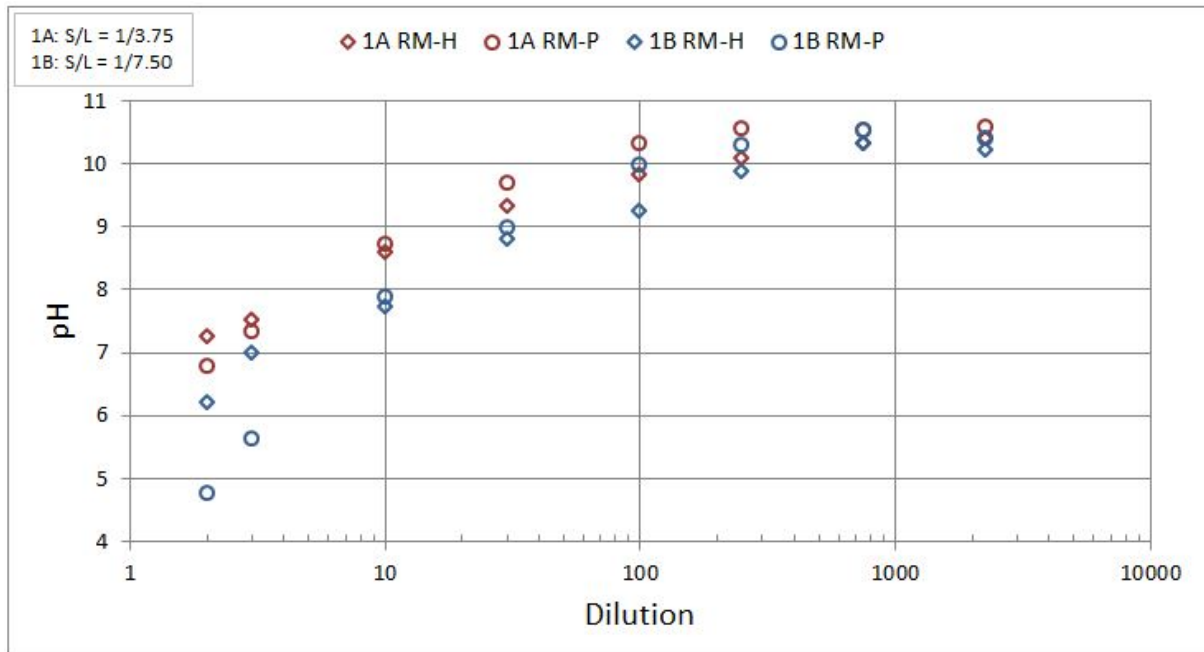


Figure 3.9: pH variation in Batch experiments 1A and 1B.

When comparing experiments 1A and 1B, it can be deduced that for dilution factors greater than or equal to 1/250, the neutralization effect on the leachate is practically the same for both amounts of solid, also the difference in pH between the two experiments reduces the more dilute the sample is.

Effect of S/L and initial concentration (C_0) in the final concentration (C_d)

Figure 3.10 and Figure 3.11 show the variation of the final concentration (C_d) with the initial concentration (C_0) of the pollutant and with the S/L (1A: S/L=1/3.75 and 1B: S/L=1/7.50). For this, nine polluting elements present in the PGL in high concentrations were selected, which were considered the most problematic due to their toxicity: arsenic (As), cadmium (Cd), chromium (Cr), copper (Cu), nickel (Ni), polonium 210 (^{210}Po), thorium (Th), uranium (U) and zinc (Zn). The relationship $C_d=C_0$ (neither sorption nor desorption occurs) is also shown in a dashed line, which allows to distinguish for which experiments the final concentration decreases with respect to the initial one (points below the dashed line), that is, the contaminant was adsorbed by the solid or precipitated, and for which experiments the concentration increases (points above the dashed line), that is, this contaminant is being released from the solid to the liquid phase. A total of 16 experiments were performed with each solid (8 from experiment A and 8 from B), some

plots show fewer points because the ICP analysis results were below the detection limit.

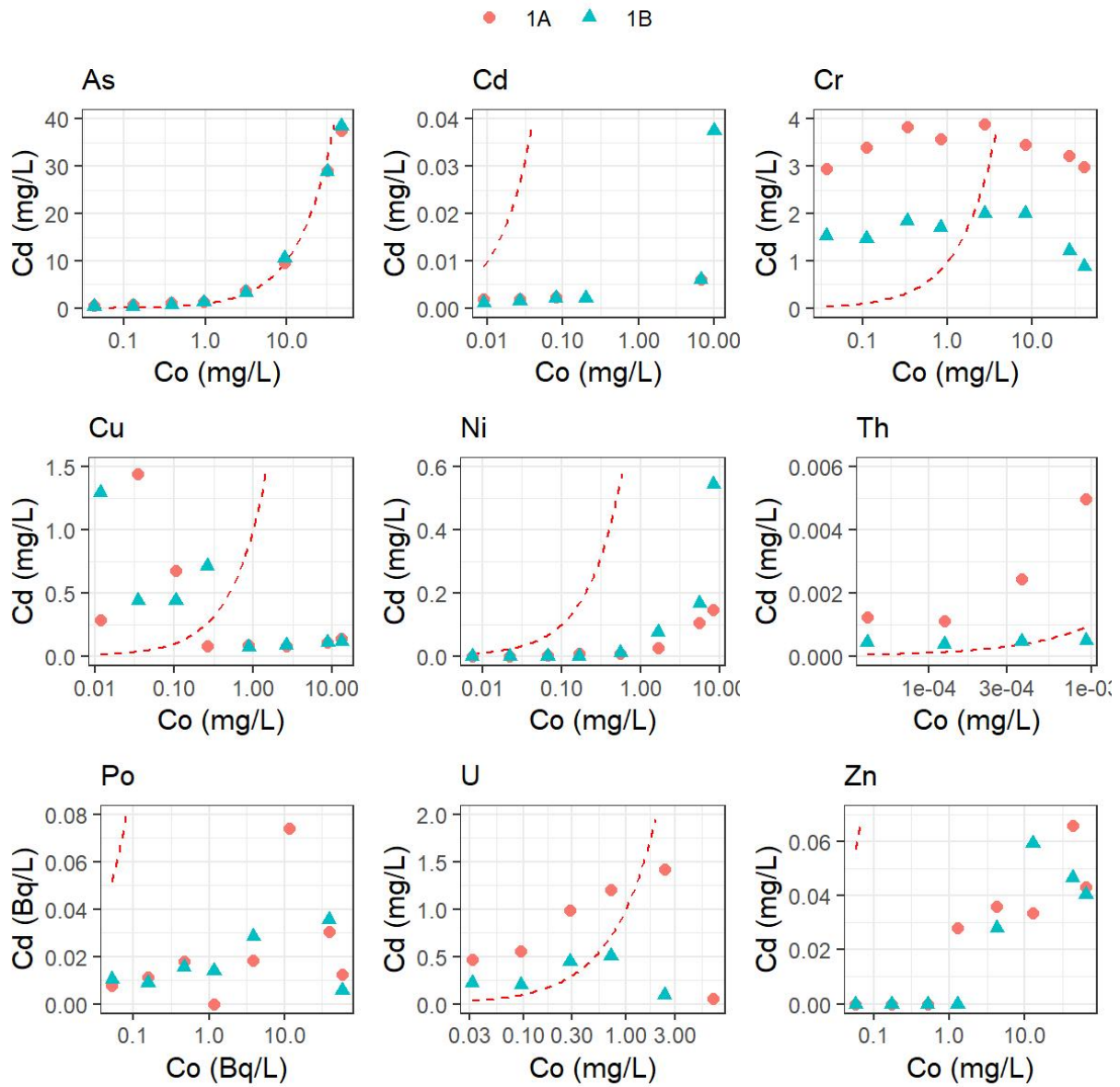


Figure 3.10: Effect of initial adsorbate concentration (C_0) and amount of solid on the final concentration (C_d) of contaminants from aqueous solution by the RM-H. The dashed line represents $C_d=C_0$.

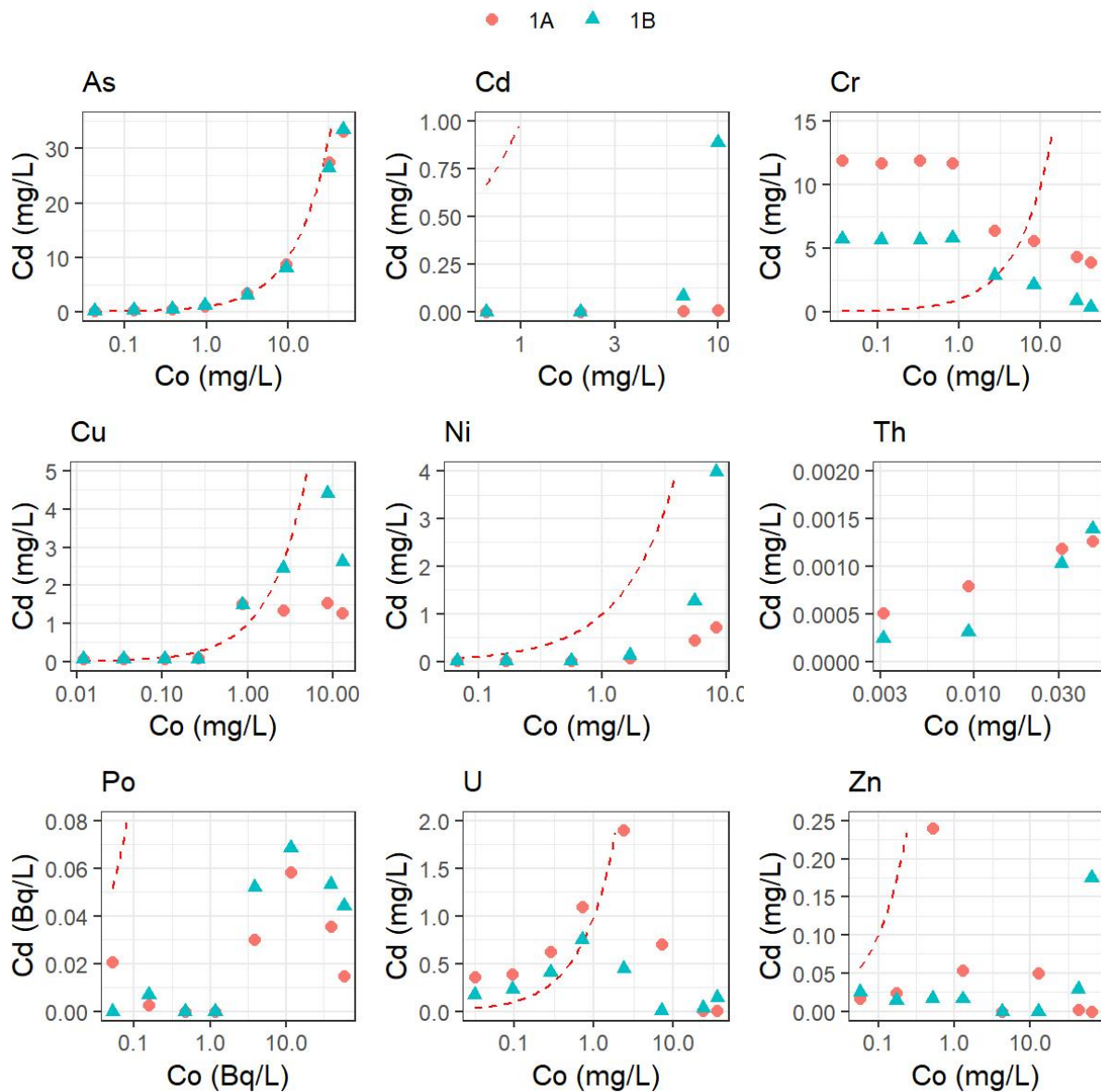


Figure 3.11: Effect of initial adsorbate concentration (C_0) and amount of solid on the final concentration (C_d) of contaminants from aqueous solution by the RM-P. The dashed line represents $C_d=C_0$.

The behaviors obtained were different for each element analyzed. In the case of As, for both RM-H and RM-P, the concentration varies very little after 24 hours of contact with the solid, the greatest variation is observed for the three highest concentrations, in which a reduction of up to 22 % with RM-H and 31 % with RM-P occurs. No difference is observed in the results with the variation of the S/L. This element is the one that had the least interaction with the red mud of all those studied.

For Cd, a significant reduction in the final concentration with respect to the initial, between 77 % and 100 % of RE, was obtained in all cases. For RM-H there was no difference in the results with the amount of solid added, while with RM-P, in the more concentrated solution of PGL the concentration of Cd is reduced less with the greater amount of solid (91 %) than with the lower (100 %).

Cr had a different behavior than expected, since for both RM-H and RM-P, the removal efficiency was higher for the lower S/L in all initial concentrations. In addition, there was an increase in the concentration of Cr after 24 h of contact with the solid in the experiments with lower initial concentration, and the best removal efficiencies occur for the most concentrated PGL solutions (up to 98 % RE with RM-H and 99 % RE with RM-P). This behavior can be explained since both red mud have a high Cr content, with the added concentration in these experiments being up to 144 mg/L in RM-H and 400 mg/L in RM-P, while the Cr concentration in the PGL is 82 mg/L. The dissolution of part of these high amounts of Cr is likely what produces an increase in its concentration in the liquid phase, and this dissolution is more easily produced for experiments with higher DF that contain fewer ions in solution.

Something similar happens with Cu, for which the highest RE occur in the highest concentrations. For RM-H, in the experiments with the highest DF, an increase in the concentration of Cu occurs after the contact time, while for the four experiments with the highest concentration, a RE between 90 % and 99 % was achieved. With RM-P on the other hand, the Cu concentration remains almost constant for the lower C_0 , while for the three highest C_0 RE between 7 % and 90 % were achieved. In the same way as with Cr, RM-H has a high content of Cu in relation to PGL (27 mg/L on average in RM-H and 26 mg/L in PGL), which means that for high dilutions, part of the Cu that was added in the solid dissolves to the liquid phase.

Ni suffered very high removals for all experiments, between 93 % and 100 % with RM-H and between 52 % and 98 % with RM-P. It is also observed that there is no noticeable effect of the variation of S/L, except for the experiment with the highest C_0 , where the final concentration decreases from 0.5 mg/L to 0.1 mg/L for the highest S/L with RM-H and from 4 mg/L to 0.7 mg/L with RM-P.

In the case of Th, results were only obtained from the experiments with the lowest C_0 for RM-H and the highest C_0 for RM-P. For the experiments with RM-H, there was generally an increase in the final concentrations compared to the initial ones and the RE were better for the lower S/L. In the experiments with RM-P a high RE was achieved, between 84 % and 97 % and a similar result for the two S/L.

For both Po and Zn, high RE are achieved with both solids, for Po between 80 % and 100 % with RM-H and between 60 % and 100 % with RM-P, and for Zn between 98 % and 100 % with RM-H and between 54 % and 100 % with RM-P. For neither of the two elements there was a considerable difference in the results when varying the S/L. These two elements are found in very high concentrations in the PGL (129 mg/L of Zn and 117 Bq/L of ^{210}Po) but in low concentration in the solid, which explains their high efficiency.

The behavior of U was similar to that of Cr since the RE were higher for the lower S/L in the two solids, in addition to the fact that for the experiments with more dilute solutions of PGL the concentration of U increased with respect to the initial one, while for those with a more concentrated solution, the concentration decreases with both solids, reaching an RE of 99 % with RM-H and 100 % with RM-P. In the case of U, despite the fact that its concentration in the solids is not as high as that of other contaminants (between 2 and 4 mg/L were added in the experiments with RM-H and between 1 and 2 mg/L in experiments with RM-P), these concentrations are high compared to those present in the liquid phase of experiments with higher DF (less than 1 mg/L). This could cause that instead of adsorption of the U in solution, a dilution of part of the U present in the solid occurred.

In summary, the behavior of the studied elements can be divided in three groups:

- i Conservative elements (As), which do not considerably vary their concentration in solution ($C_d \approx C_0$).
- ii Elements with efficient removal for all values of C_0 (Cd, Ni, Po and Zn), whose concentration in solution decreases in all the experiments ($C_d < C_0$).
- iii Elements with variable removal efficiencies depending on the C_0 (Cr, Cu, Th and U), which increase their concentration in solution for low values of C_0 but have a

high removal efficiency for values of C_0 close to that of the original undiluted PGL. Regarding the comparison of the two red muds, all the elements had a similar behavior with RM-H and RM-P. In general, RM-H had a better performance than RM-P, since for the experiment with the highest C_0 , RM-H was more efficient in the removal of Cd, Cr, Cu, Ni and U, while RM -P was only more efficient in the removal of As, for Po and Zn RE close to 100 % were obtained with both solids.

Effect of initial concentration in the partition coefficient (K_d isotherms)

The concentration in the solid phase (C_s) of RM-H and RM-P versus the final contaminant concentration in equilibrium (C_d) is shown in Figure 3.12 and Figure 3.13. Only the values of $C_s > 0$ are shown since they are the ones that make physical sense, that is, all the results in which the final equilibrium concentration in solution is higher than the initial one, cannot be represented in these plots. These plots represent the K_d isotherms and were made in order to study if they fit any of the three adsorption isotherms that are typically used to describe the interaction between an adsorbent and an adsorbate at equilibrium: the Langmuir (Equation 1.3), Freundlich (Equation 1.5) and Dubinin–Radushkevich (DR) (Equation 1.7) isotherm models.

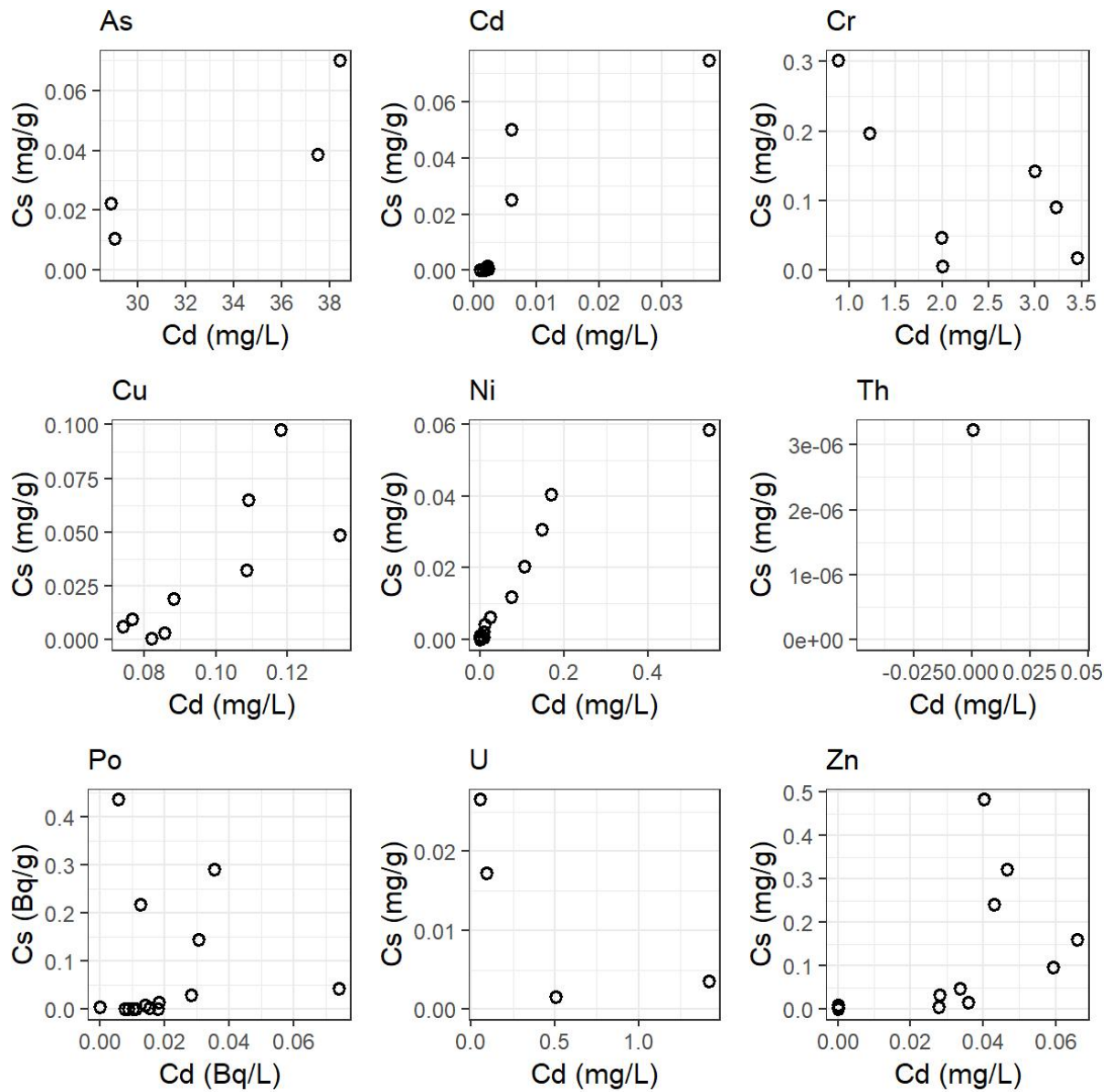


Figure 3.12: Effect of initial adsorbate concentration on the removal of contaminants from aqueous solution by the RM-H.

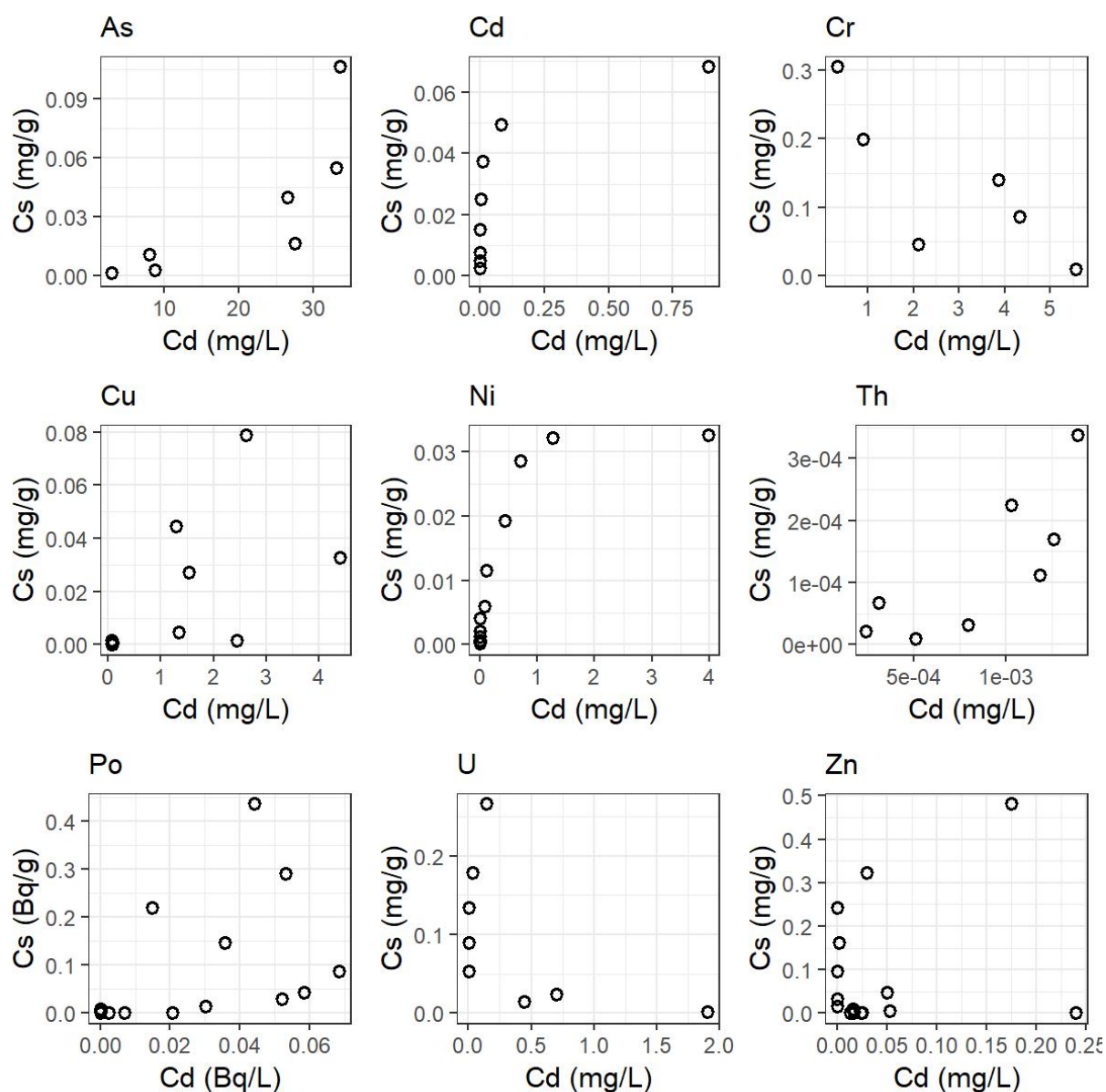


Figure 3.13: Effect of initial adsorbate concentration on the removal of contaminants from aqueous solution by the RM-P.

From a visual analysis of the plots of C_s vs C_d , it was determined that the elements that could potentially fit some of the models (mainly because they have a clear trend of $C_s \propto C_d$ in addition to having at least 4 values) were Cd and Ni with both RM-H and RM-P. These data were adjusted with the three models mentioned, comparing the goodness of fit with the coefficient R^2 and taking the best in each case, which is shown in Figure 3.14. The model that best fitted the Cd isotherms was the DR model, being the fit only satisfactory for RM-P, with $R^2=0.73$. For Ni, its interaction with RM-H fits

the Freundlich model with $R^2=0.97$, while with RM-P it better fits the DR model with $R^2=0.87$, but it also presents a good fit with the Freundlich model with a slightly lower R^2 of 0.83 (Table 3.9).

From the model that best fits the K_d isotherm of each element, and the fit parameters, certain characteristics can be inferred about the adsorption mechanism of the pollutant to the red mud. The mean free energy (E_a , which is the energy per molecule of adsorbate needed to remove a molecule from its location in the sorption space to the infinity (Dada 2012)) can be approximated from the parameter K_D of the DR model, and it is often used to distinguish the dominant adsorption mechanism, with E_a values < 8 kJ/mol, 8–16 kJ/mol, and > 16 kJ/mol referring to physical, ion exchange, and chemical adsorption, respectively (Sun et al. 2022). In this case, adsorption free energy was calculated from the DR model, with Equation 1.9 (Xiong et al. 2021).

This resulted in values of E_a for Cd with RM-P of 7976 kJ/mol, which is > 16 kJ/mol and indicates that the main adsorption mechanism of Cd with red mud is chemical adsorption.

The adsorption of Ni by both RM-H and RM-P seemed to be well described by the Freundlich model, this indicates that the adsorption to the red muds is multilayered and the adsorption surface is heterogeneous (Yu et al. 2021). This is in agreement with the work of Zouboulis and Kydros (2007) who also found that the adsorption of Ni with red mud presented a good fit with the Freundlich model. According to Treybal (1981), the magnitude of the parameter N is related to the favorability of the adsorption process. N values in the range 2–10 represent good, 1–2 moderately difficult, and less than 1 a poor adsorptive potential. In this study, the values of N obtained for RM-H and RM-P (0.97 and 0.67 respectively) indicate a poor adsorption process of Ni to the red mud. Smaller values of $1/N$ are associated to the formation of relatively strong bonds between the adsorbate molecules and adsorbent (To et al. 2017), so in this case, the high values of $1/N$ indicate a weak interaction.

In the case of RM-P, the adsorption of Ni can also be explained by the DR model, with a value of $E_a=4640$ kJ/mol, which indicates that as with Cd, the adsorption of Ni to RM-P is mainly chemical.

The fact that several elements did not fit correctly to any adsorption model may be related

to the fact that in the batch experiments carried out, in addition to varying the initial concentration, by varying the DF of the PGL, the initial and final pH did not remain constant in each experiment. The adsorption/precipitation processes of some elements (such as As, Cr, Cu and U) has shown to significantly vary with pH variations (Papaslioti et al. 2018a, Nadaroglu et al. 2010, White et al. 2003), which includes an extra variable that is not considered in the adsorption isotherm models.

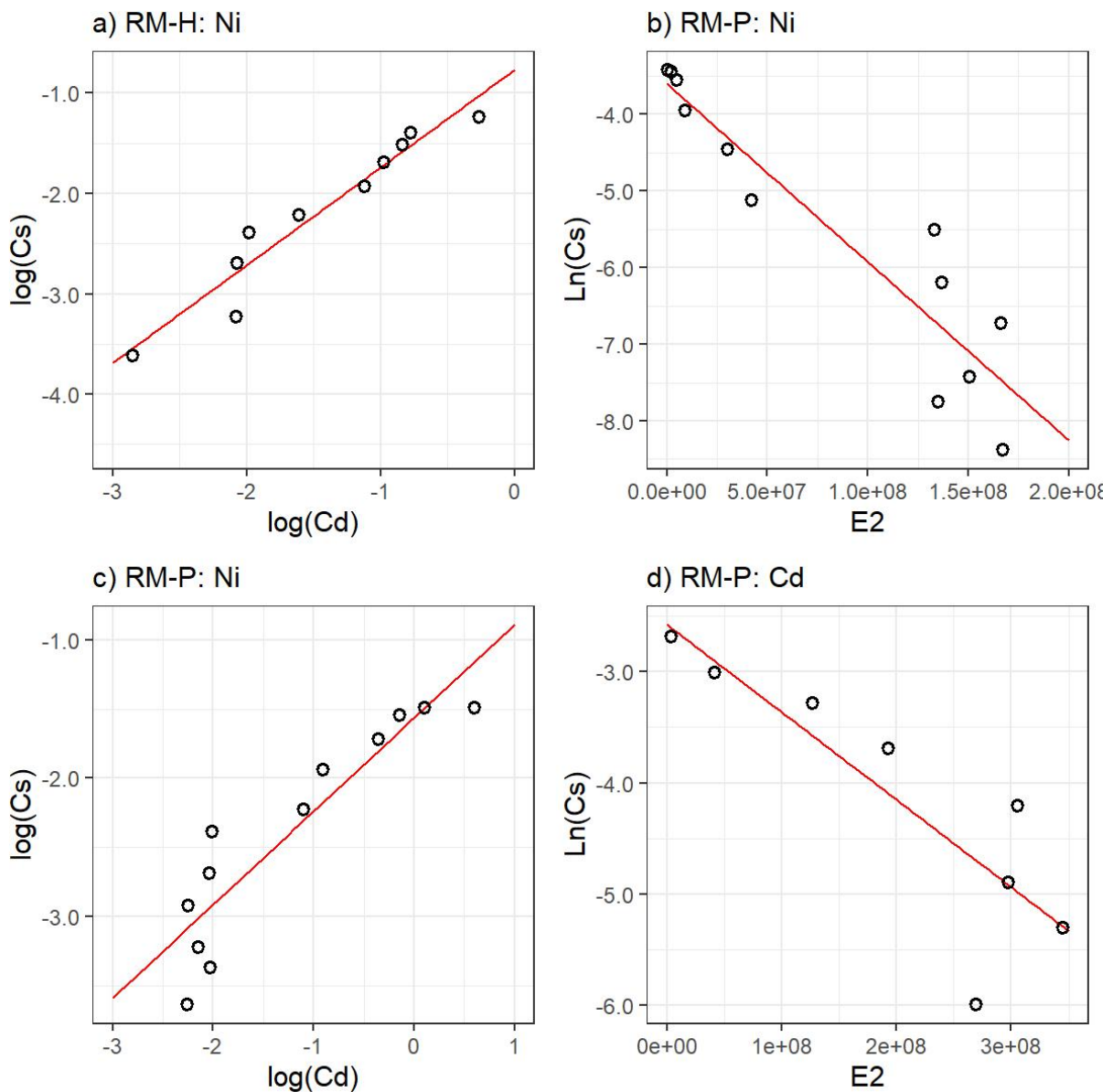


Figure 3.14: Linear fit of Ni and Cd isotherms to Freundlich model (a and c) and DR model (b and d).

Table 3.9: Parameters of the best fit model of the Cd and Ni isotherms with RM-H and RM-P.

Solid	RM-H	RM-P		
Element	Ni	Cd	Ni	Ni
Model	Freundlich	DR	DR	Freundlich
R ²	0.93	0.73	0.87	0.83
K _F (mg/g)	(17.0±0.2)·10 ⁻²	-	-	(2.7±0.1)·10 ⁻²
N	0.97±0.09	-	-	0.67±0.10
K _D (mol ² /kJ ²)	-	(7.9±0.2)·10 ⁻⁹	(2.3±0.3)·10 ⁻⁸	-
C _m (mg/g)	-	(7.6±3.4)·10 ⁻²	(2.7±0.8)·10 ⁻²	-

3.4.2 Batch experiment 2

In this experiment, the variation of pH with contact time was studied, for this, the conditions that were held constant were:

- Solid mass = 20 g
- PGL dilution mass = 150 g
- Dilution factor
 - * 2A: DF = 1/100 (initial pH = 2.5)
 - * 2B: DF = 1/10 (initial pH = 2.0)

This experiment was first performed for DF=1/100 (2A) since, according to the results of the Batch experiment 1, it is the dilution factor from which the maximum pH values can be reached. The variation of the contact time did not produce great differences in the final pH obtained for this DF (Figure 3.15), especially for RM-P for which there is only a difference in pH of 0.1 between the contact time of 15 minutes and that of 24 hours, for RM-H this difference is of 0.6.

The lowest final pH corresponded to the shortest contact time (15 min) and the highest pH to the longest contact time (24 h), however the intermediate values did not fit any

particular relationship. As it was expected from the results of experiment 1B with dilution factor 1/100, the pH reached with RM-P in experiment 2 is slightly higher than with RM-H for all contact times. This shows that for a DF=1/100, the PGL neutralization is almost instantaneous.

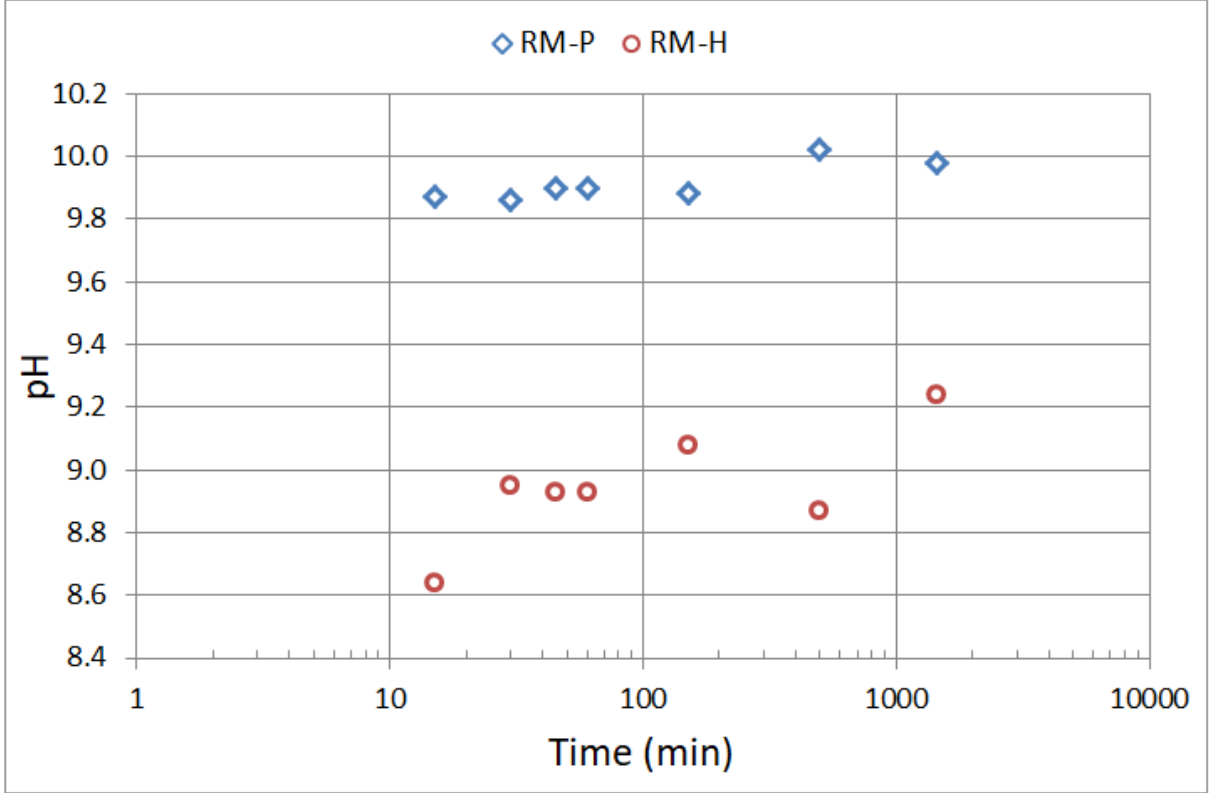


Figure 3.15: pH variation with time in Batch experiment 2A with DF=1/100.

The same experiment was then performed for a DF=1/10 (2B). In this case, a clear variation of pH with time can be observed (Figure 3.16). The results show a logarithmic dependence of pH with contact time, which follows the relationships: $pH = (26.5 \pm 0.6) \times 10^{-2} \ln(t) + (58.2 \pm 0.3) \times 10^{-1}$ ($R^2=0.991$) for RM-H and $pH = (27.8 \pm 0.8) \times 10^{-2} \ln(t) + (57.8 \pm 0.3) \times 10^{-1}$ ($R^2=0.991$) for RM-P. This adjustment is not correct when time tends to infinity, since the pH would continue to increase, but it is an adequate adjustment for the range of contact time analysed. The uncertainties obtained were very low and both residuals give compatible fits, that is, they can be considered equal within the experimental uncertainties. For this dilution factor, the effect on the pH of the solution is practically the same with both red muds. It can be stated that the contact time necessary to neutralize the solution (of DF = 1/10, with S/L = 1/7.50), that is, to

3 RESULTS AND DISCUSSION

reach a pH equal to 7, is approximately 85 minutes, and the pH does not continue to increase significantly after this time, reaching a final value of 7.7 (RM-H) and 7.9 (RM-P) after 24 hours.

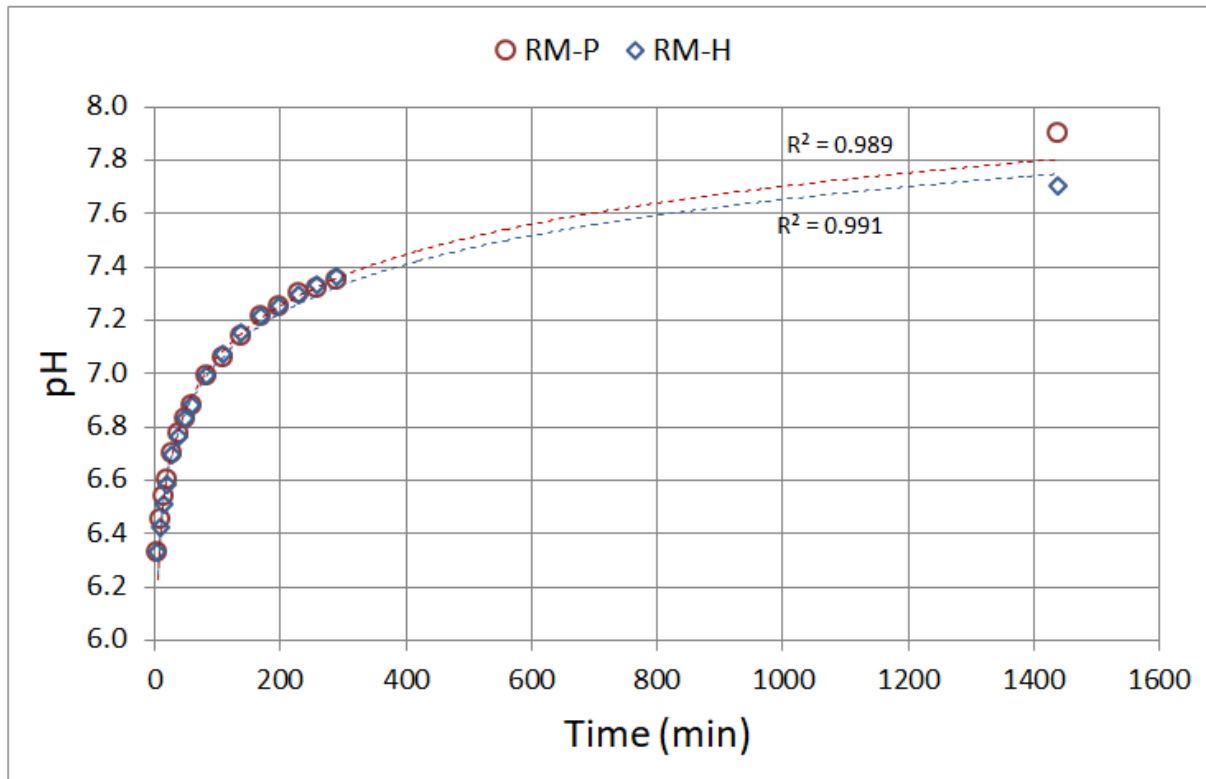


Figure 3.16: pH variation with time in Batch experiment 2B with DF=1/10.

4 Conclusions

In this work, a characterization of alkaline waste materials from the aluminum industry (red mud) has been carried out, as well as an analysis of its capacity for the neutralization and decontamination of phosphogypsum leachates. This section summarizes the most significant conclusions that were obtained.

1. The phosphogypsum leachates were chemically characterized, showing that their main composition is phosphates ($\approx 10^5$ ppm), fluorides ($\approx 10^3$ ppm) and sulfates ($\approx 10^3$ ppm), in addition to containing high concentrations of the radioelements U (71 ppm) and ^{210}Po (117 Bq/L) and metals such as As (100 ppm), Cd (20 ppm), Cr (80 ppm), Cu (30 ppm), Fe (200 ppm), Mn (60 ppm), Ni (20 ppm) and Zn (100 ppm), all 4 to 5 orders of magnitude above natural seawater values.
2. Three alkaline solid wastes were characterized, two red muds from the aluminium industry and one domestic ash. All three have an alkaline pH between 10.7 and 12.2. The red muds are mainly composed of Fe (15-30 %), Al (10-12 %), Na (5-9 %), Si (3-7 %), Ti (4 %) and Ca (1-4 %) forming oxides and hydroxides, while the ashes are mainly composed of CaCO_3 (50 %), being for the three between 35 and 50 % of its composition amorphous.
3. The acid neutralizing capacity of each solid was calculated from the results of titration curves with HNO_3 , H_3PO_4 and PGL. This showed that the domestic ash has a higher neutralization capacity in all cases, while the red muds have a very similar capacity.
4. Titration curves of the PGL with the three solids showed that all of them have the capacity of increasing the PGL pH until acceptable values of discharge to the estuary (6.8-7.3). Domestic ashes were the most effective as a lower solid to liquid ratio (0.22) was needed to achieve the maximum pH, while for RM-H and RM-P similar ratios were used (0.43 and 0.54 respectively).
5. The resulting liquid from the titration curves of the solid with PGL was analyzed to determine the removal efficiency of each solid for the main pollutants. The results showed that ashes were effective for the removal of more contaminants up to a value permitted by regulations. RM-H achieved high removal efficiencies in most elements

(close to 100 %), failing to comply with regulated values only for As (46 ppm), Cd (0.02 ppm), Cr (6 ppm) and P (1900 ppm), even though the final concentrations were significantly lower than the original ones. These elements are partially conservative and their RE order was Cd (100 %) > Cr (93 %) > P(92 %) > As (52 %). The rest of the studied elements achieved final concentration values that complied with the limits (Al: 1 ppm, Cu: 0.16 ppm, Fe: 1 ppm, Mn: 0.02 ppm, Ni: 0.2 ppm, Pb: 0.01 ppm, Ti: 0.04 ppm, Zn: 0.08 ppm). RM-P failed to efficiently remove As (43 ppm), Cd (0.02 ppm), Cr (20 ppm), Cu (6 ppm), Ni (2 ppm), P (3200 ppm) and Ti (23 ppm), with RE order: Cd (100 %) > Ni (89 %) > P (86 %) > Cu (78 %) > Ti (76 %) > Cr (75 %) > As (55 %), even though remotions of over 55 % occurred for all these elements, whilst the rest of the analyzed elements satisfactorily reduced their concentration (Al: 0.7 ppm, Fe: 0.1 ppm, Mn: 0.03 ppm, Pb: 0.02 ppm, Zn: 0.4 ppm).

6. Batch experiments were carried out to study the sorption of contaminants present in PGL to red mud. This showed that As was the most conservative of the studied elements, since its concentration does not suffer reductions of more than 31 %. It was also observed, that for some elements that are present in high concentrations in the red mud (Cr, Cu, Th and U), when PGL dilution is high (DF over 1/100) their final concentration in solution rises instead of decreasing after the experiment. For the rest of the elements (Cd, Ni, Po and Zn) the final concentration decreases after the interaction with red mud. The results for Cd had an acceptable fit ($R^2 = 0.73$) to the Dubinin-Radushkevich adsorption isotherm model for RM-P, suggesting that the main adsorption mechanism for Cd to red mud is chemical adsorption. The results of Ni fitted ($R^2 = 0.83-0.97$) the Freundlich adsorption isotherm model, which indicates that the adsorption mechanism is multilayered, the adsorption surface of red mud is heterogeneous and that the interaction between Ni and the adsorbent is weak.
7. Batch experiments also demonstrated that the variation of pH with time for PGL with a DF = 1/100 occur very rapidly, remaining the pH practically the same (8.5-10) after the 5 minutes of contact time. When PGL is less diluted (DF = 1/10) pH increases rapidly during the first hour approximately until neutral pH and then continues to increase slightly until equilibrium values between 7.5 and 8.

8. The results obtained show that red mud could potentially be used as an alkaline agent in a passive treatment to improve the quality of phosphogypsum leachates, since both the studied residues achieve leachate neutralization and removal or high reductions of most contaminants. Future work can be carried out on the study of a complementary treatment with a chemical reagent, such as $\text{Ca}(\text{OH})_2$, for the removal of the fraction of contaminants that cannot be eliminated with the red mud treatment. This would mean both a reduction in material costs and an environmental advantage by giving this industrial waste a productive use. The behavior of K_d for different PGL dilutions was studied, which could be useful as input data for a future permeable reactive barrier design for the PLG treatment.

References

- Absi, A. et al. (2004). Self-cleaning in an estuarine area formerly affected by ^{226}Ra anthropogenic enhancements. In: *Science of the Total Environment* 329.1-3, pp. 183–195. ISSN: 00489697. DOI: 10.1016/j.scitotenv.2004.03.001.
- Agrawal, Archana, K. Sahu, and B. Pandey (Oct. 2004). A comparative adsorption study of copper on various industrial solid wastes. In: *AIChE Journal* 50, pp. 2430–2438. DOI: 10.1002/aic.10206.
- Alkan, Gözde et al. (2017). A mineralogical assessment on residues after acidic leaching of bauxite residue (Red mud) for titanium recovery. In: *Metals* 7.11. ISSN: 20754701. DOI: 10.3390/met7110458.
- Ames, L. L. et al. (1982). Sorption of Uranium and Cesium by Hanford Basalts and Associated Secondary Smectite. In: *Chemical Geology* 35:205-225, pp. 205–225. URL: <http://eprints.uanl.mx/5481/1/1020149995.PDF>.
- Anon (1967). Removal of Iron from US Bauxite Liquor Using Red Mud — Derived from Caribbean Aluminous Ores. (Reynolds Metals Co). In.
- Apak, Reşat et al. (1998). Heavy metal cation retention by unconventional sorbents (red muds and fly ashes). In: *Water Research* 32.2, pp. 430–440. ISSN: 00431354. DOI: 10.1016/S0043-1354(97)00204-2.
- Bai, Bing et al. (2022). The remediation efficiency of heavy metal pollutants in water by industrial red mud particle waste. In: *Environmental Technology and Innovation* 28, p. 102944. ISSN: 23521864. DOI: 10.1016/j.eti.2022.102944. URL: <https://doi.org/10.1016/j.eti.2022.102944>.
- Blasco, M. et al. (2016). Polonium behaviour in reservoirs potentially affected by acid mine drainage (AMD) in the Iberian Pyrite Belt (SW of Spain). In: *Journal of Environmental Radioactivity* 152, pp. 60–69. ISSN: 18791700. DOI: 10.1016/j.jenvrad.2015.11.008.
- BOE (2001). REAL DECRETO 783/2001, de 6 de julio, por el que se aprueba el Reglamento sobre protección sanitaria contra radiaciones ionizantes. In: *Boletín Oficial del Estado*, pp. 1–37.
- Bogush, Anna A. et al. (2020). Biomass Ashes for Acid Mine Drainage Remediation. In: *Waste and Biomass Valorization* 11.9, pp. 4977–4989. ISSN: 1877265X. DOI: 10.1007/s12649-019-00804-9. URL: <https://doi.org/10.1007/s12649-019-00804-9>.
- Bolivar, J. P., R. García-Tenorio, and M. García-León (1996). On the fractionation of natural radioactivity in the production of phosphoric acid by the wet acid method. In: *Journal of Radioanalytical and Nuclear Chemistry* 214.2, pp. 77–88. ISSN: 02365731. DOI: 10.1007/BF02164808.
- Bolívar, J. P. et al. (2009). Behaviour and fluxes of natural radionuclides in the production process of a phosphoric acid plant. In: *Applied Radiation and Isotopes* 67.2, pp. 345–356. ISSN: 09698043. DOI: 10.1016/j.apradiso.2008.10.012.

REFERENCES

- Canti, M. G. (2003). Aspects of the chemical and microscopic characteristics of plant ashes found in archaeological soils. In: *Catena* 54.3, pp. 339–361. ISSN: 03418162. DOI: 10.1016/S0341-8162(03)00127-9.
- Chen, Zheng et al. (2022). Effectiveness and mechanism of uranium adsorption on size-graded red mud. In: *Environmental Research* 212.PD, p. 113491. ISSN: 10960953. DOI: 10.1016/j.envres.2022.113491. URL: <https://doi.org/10.1016/j.envres.2022.113491>.
- CSN (2011). Instruction IS-33, 21 December 2011, from the Nuclear Safety Council on radiological criteria for protection against the natural radiation (In Spanish). In.
- Dabrowski, A. (2001). Adsorption - From theory to practice. In: *Advances in Colloid and Interface Science* 93.1-3, pp. 135–224. ISSN: 00018686. DOI: 10.1016/S0001-8686(00)00082-8.
- Dada, A.O (2012). Langmuir, Freundlich, Temkin and Dubinin–Radushkevich Isotherms Studies of Equilibrium Sorption of Zn 2+ Unto Phosphoric Acid Modified Rice Husk. In: *IOSR Journal of Applied Chemistry* 3.1, pp. 38–45. DOI: 10.9790/5736-0313845.
- Decreto 109/2015 (2015). 17 de marzo, por el que se aprueba el Reglamento de Vertidos al Dominio Público Hidráulico y al Dominio Público Marítimo-Terrestre de Andalucía (BOJA nº 89 de 12/05/2015).
- Dubinin, M. M. (1947). The Equation of the Characteristic Curve of Activated Charcoal. In: *Proceedings of the USSR Academy of Sciences* 55, pp. 327–329.
- Dursun, Sukru et al. (2008). Removal of chromate from aqueous system by activated red-mud. In: *Asian Journal of Chemistry* 20.8, pp. 6473–6478. ISSN: 09707077.
- EPA (1999). Understanding Variation in Practice. In: *Understanding variation in partition coefficient, Kd, values 1*.
- European Parliament (2014). Council Directive 2013/59/Euratom of 5 December 2013 laying down basic safety standards for protection against the dangers arising from exposure to ionising radiation, and repealing Directives 89/618/Euratom, 90/641/Euratom, 96/29/Euratom, 97/43/Euratom a. In: *Off J Eur Commun L13* December 2003, pp. 1–73.
- Freundlich, H. (1926). Colloid and Capillary Chemistry. In: *Methuen, London, England*.
- García-García, R. et al. (2020). Speciation diagrams in some metal ions-H₃PO₄ system. In: *International Journal of Electrochemical Science* 15, p. 3607. ISSN: 14523981. DOI: 10.20964/2020.04.04.
- Giles, Charles H, David Smith, and Alan Huitson (1974). A general treatment and classification of the solute adsorption isotherm. I. Theoretical. In: *Journal of Colloid and Interface Science* 47.3, pp. 755–765. ISSN: 0021-9797. DOI: [https://doi.org/10.1016/0021-9797\(74\)90252-5](https://doi.org/10.1016/0021-9797(74)90252-5). URL: <https://www.sciencedirect.com/science/article/pii/0021979774902525>.

REFERENCES

- Gouider, Mbarka, Mongi Feki, and Sami Sayadi (2009). Separative recovery with lime of phosphate and fluoride from an acidic effluent containing H₃PO₄, HF and/or H₂SiF₆. In: *Journal of Hazardous Materials* 170.2-3, pp. 962–968. ISSN: 03043894. DOI: 10.1016/j.jhazmat.2009.05.067.
- Gräfe, M., G. Power, and C. Klauber (2011). Bauxite residue issues: III. Alkalinity and associated chemistry. In: *Hydrometallurgy* 108.1-2, pp. 60–79. ISSN: 0304386X. DOI: 10.1016/j.hydromet.2011.02.004. URL: <http://dx.doi.org/10.1016/j.hydromet.2011.02.004>.
- Guerrero, J. L. et al. (2021). Seasonal evolution of natural radionuclides in two rivers affected by acid mine drainage and phosphogypsum pollution. In: *Catena* 197. November 2020, p. 104978. ISSN: 03418162. DOI: 10.1016/j.catena.2020.104978. URL: <https://doi.org/10.1016/j.catena.2020.104978>.
- Günay, Ahmet, Ertan Arslankaya, and Ismail Tosun (2007). Lead removal from aqueous solution by natural and pretreated clinoptilolite: Adsorption equilibrium and kinetics. In: *Journal of Hazardous Materials* 146.1-2, pp. 362–371. ISSN: 03043894. DOI: 10.1016/j.jhazmat.2006.12.034.
- Heviánková, Silvie et al. (2014). Acid mine drainage treatment by ash from wooden chip combustion: Study of mine water composition in dependence on the ash dose and duration of mutual interaction. In: *Carpathian Journal of Earth and Environmental Sciences* 9.2, pp. 159–170. ISSN: 1844489X.
- Hind, Andrew R, Suresh K Bhargava, and Stephen C Grocott (1999). The surface chemistry of Bayer process solids : a review. In: 146, pp. 359–374.
- IAEA (2013). Radiation Protection and Management of NORM Residues in the Phosphate Industry. In: *Safety Reports Series No. 78* 78, p. 288. ISSN: 03014207.
- Khairul, M. A., Jafar Zanganeh, and Behdad Moghtaderi (2019). The composition, recycling and utilisation of Bayer red mud. In: *Resources, Conservation and Recycling* 141. November 2018, pp. 483–498. ISSN: 18790658. DOI: 10.1016/j.resconrec.2018.11.006. URL: <https://doi.org/10.1016/j.resconrec.2018.11.006>.
- Khaitan, Sameer, David A. Dzombak, and Gregory V. Lowry (2009). Chemistry of the acid neutralization capacity of bauxite residue. In: *Environmental Engineering Science* 26.5, pp. 873–881. ISSN: 10928758. DOI: 10.1089/ees.2007.0228.
- Koukouzas, Nikolaos et al. (2009). Quantitative evaluation of minerals in fly ashes of biomass, coal and biomass-coal mixture derived from circulating fluidised bed combustion technology. In: *Journal of Hazardous Materials* 169.1-3, pp. 100–107. ISSN: 03043894. DOI: 10.1016/j.jhazmat.2009.03.116.
- Kumarasinghe, Udayagee et al. (2018). Evaluation of applicability of filling materials in permeable reactive barrier (PRB) system to remediate groundwater contaminated with Cd and Pb at open solid waste dump sites. In: *Process Safety and Environmental*

REFERENCES

- Protection* 120.September, pp. 118–127. ISSN: 09575820. DOI: 10.1016/j.psep.2018.09.003. URL: <https://doi.org/10.1016/j.psep.2018.09.003>.
- Langmuir, I. (1919). Adsorption of gases on glass, mica and platinum. In: *Journal of the American Chemical Society* 40.1914, pp. 1361–1403.
- Lawrence, Richard W. and Michael Scheske (1997). A method to calculate the neutralization potential of mining wastes. In: *Environmental Geology* 32.2, pp. 100–106. ISSN: 09430105. DOI: 10.1007/s002540050198.
- Liu, Yanju and Ravi Naidu (2014). Hidden values in bauxite residue (red mud): Recovery of metals. In: *Waste Management* 34.12, pp. 2662–2673. ISSN: 18792456. DOI: 10.1016/j.wasman.2014.09.003. URL: <http://dx.doi.org/10.1016/j.wasman.2014.09.003>.
- Macián, Concepción (Jan. 2007). Caracterización de los procesos de eliminación de metales de aguas ácidas utilizando magnesia caústica. Aplicación al tratamiento in situ. In: Maresca, A., J. Hyks, and T. F. Astrup (2017). Recirculation of biomass ashes onto forest soils: ash composition, mineralogy and leaching properties. In: *Waste Management* 70, pp. 127–138. ISSN: 18792456. DOI: 10.1016/j.wasman.2017.09.008. URL: <https://doi.org/10.1016/j.wasman.2017.09.008>.
- Mas, J. L. et al. (2006). An assay on the effect of preliminary restoration tasks applied to a large TENORM wastes disposal in the south-west of Spain. In: *Science of the Total Environment* 364.1-3, pp. 55–66. ISSN: 00489697. DOI: 10.1016/j.scitotenv.2005.11.006.
- McLachlan, R. et al. (1998). Micro Reform – Impacts on Firms: Aluminium Case Study. Research paper / Industry Commission. Industry Commission. ISBN: 9780646335506. URL: <https://books.google.es/books?id=L5zDAAAACAAJ>.
- Millán-Becerro, Ricardo et al. (2019). Assessment of metals mobility during the alkaline treatment of highly acid phosphogypsum leachates. In: *Science of the Total Environment* 660, pp. 395–405. ISSN: 18791026. DOI: 10.1016/j.scitotenv.2018.12.305. URL: <https://doi.org/10.1016/j.scitotenv.2018.12.305>.
- Millán-Becerro, Ricardo et al. (2020). Design and optimization of sustainable passive treatment systems for phosphogypsum leachates in an orphan disposal site. In: *Journal of Environmental Management* 275.April. ISSN: 10958630. DOI: 10.1016/j.jenvman.2020.111251.
- Millán-Becerro, Ricardo et al. (2021). Combined procedure of metal removal and recovery of technology elements from fertilizer industry effluents. In: *Journal of Geochemical Exploration* 221.September 2020. ISSN: 03756742. DOI: 10.1016/j.gexplo.2020.106698.
- Nadaroglu, Hayrunnisa, Ekrem Kalkan, and Nazan Demir (2010). Removal of copper from aqueous solution using red mud. In: *Desalination* 251.1-3, pp. 90–95. ISSN: 00119164. DOI: 10.1016/j.desal.2009.09.138. URL: <http://dx.doi.org/10.1016/j.desal.2009.09.138>.

REFERENCES

- Nonose, Naoko et al. (2014). Precise determination of dissolved silica in seawater by ion-exclusion chromatography isotope dilution inductively coupled plasma mass spectrometry. In: *Analytica Chimica Acta* 840, pp. 10–19. ISSN: 0003-2670. DOI: <https://doi.org/10.1016/j.aca.2014.06.018>. URL: <https://www.sciencedirect.com/science/article/pii/S000326701400751X>.
- Papaslioti, Evgenia Maria et al. (2018a). Effects of seawater mixing on the mobility of trace elements in acid phosphogypsum leachates. In: *Marine Pollution Bulletin* 127, November 2017, pp. 695–703. ISSN: 18793363. DOI: 10.1016/j.marpolbul.2018.01.001. URL: <https://doi.org/10.1016/j.marpolbul.2018.01.001>.
- Papaslioti, Evgenia Maria et al. (2018b). Stable isotope insights into the weathering processes of a phosphogypsum disposal area. In: *Water Research* 140, pp. 344–353. ISSN: 18792448. DOI: 10.1016/j.watres.2018.04.060. URL: <https://doi.org/10.1016/j.watres.2018.04.060>.
- Pérez-López, Rafael et al. (2016). Pollutant flows from a phosphogypsum disposal area to an estuarine environment: An insight from geochemical signatures. In: *Science of the Total Environment* 553, pp. 42–51. ISSN: 18791026. DOI: 10.1016/j.scitotenv.2016.02.070. URL: <http://dx.doi.org/10.1016/j.scitotenv.2016.02.070>.
- Pérez-Moreno, S. M. et al. (2018). Assessment of natural radionuclides mobility in a phosphogypsum disposal area. In: *Chemosphere* 211, pp. 775–783. ISSN: 18791298. DOI: 10.1016/j.chemosphere.2018.07.193.
- Pérez-Moreno, Silvia et al. (2022). Development of a Process for the Removal of Natural Radionuclides and Other Stable Pollutants from Acid Phosphogypsum Stacks Leachates. In: *SSRN Electronic Journal* 11, November 2022. DOI: 10.2139/ssrn.4130058.
- Pohland, H. and B. Schepers (1985). Aluminium Hydroxide with Low Impurity Esp. Iron Content Recovery - From Process Liquor by Adding Calcium Oxide or Hydroxide and Magnesium Sulphate before Pptn. In: Cited By :1, p. 11. URL: www.scopus.com.
- Qureshi, Asif et al. (2016). Potential of fly ash for neutralisation of acid mine drainage. In: *Environmental Science and Pollution Research* 23, 17, pp. 17083–17094. ISSN: 16147499. DOI: 10.1007/s11356-016-6862-3. URL: <http://dx.doi.org/10.1007/s11356-016-6862-3>.
- Rudnick, R. L. and S. Gao (2013). Composition of the Continental Crust. 2nd ed. Vol. 4. October 2017. Elsevier Ltd., pp. 1–51. ISBN: 9780080983004. DOI: 10.1016/B978-0-08-095975-7.00301-6. URL: <http://dx.doi.org/10.1016/B978-0-08-095975-7.00301-6>.
- Samal, Sneha, Ajoy K. Ray, and Amitava Bandopadhyay (2013). Proposal for resources, utilization and processes of red mud in India — A review. In: *International Journal of Mineral Processing* 118, pp. 43–55. ISSN: 03017516. DOI: 10.1016/j.minpro.2012.11.001. URL: <http://dx.doi.org/10.1016/j.minpro.2012.11.001>.

REFERENCES

- Sano, Tetsuya et al. (2013). Composition of inorganic elements and the leaching behavior of biomass combustion ashes discharged from wood pellet boilers in Japan. In: *Journal of Wood Science* 59.4, pp. 307–320. ISSN: 14350211. DOI: 10.1007/s10086-013-1337-3.
- Smolka-Danielowska, Danuta and Mariola Jabłońska (2022). Chemical and mineral composition of ashes from wood biomass combustion in domestic wood-fired furnaces. In: *International Journal of Environmental Science and Technology* 19.6, pp. 5359–5372. ISSN: 17352630. DOI: 10.1007/s13762-021-03506-9. URL: <https://doi.org/10.1007/s13762-021-03506-9>.
- Sposito, Garrison (1984). *The surface chemistry of soils* / Garrison Sposito. English. Oxford University Press ; Clarendon Press New York : Oxford [Oxfordshire], xii, 234 p. : ISBN: 019503421.
- Srikanth, Srinivasan et al. (2005). Phase constitution during Sintering of red mud and red mud-fly ash mixtures. In: *Journal of the American Ceramic Society* 88.9, pp. 2396–2401. ISSN: 00027820. DOI: 10.1111/j.1551-2916.2005.00471.x.
- Sun, Yongchang et al. (2022). Facile synthesis of Fe-modified lignin-based biochar for ultra-fast adsorption of methylene blue: Selective adsorption and mechanism studies. In: *Bioresource Technology* 344.PA, p. 126186. ISSN: 18732976. DOI: 10.1016/j.biortech.2021.126186. URL: <https://doi.org/10.1016/j.biortech.2021.126186>.
- Sutar, H. et al. (2014). Progress of red mud utilization: an overview. In: *Am.Chem.Sci.J.* 4.3. Cited By :133, pp. 255–279. URL: www.scopus.com.
- Thomas, R (2001). A beginner's guide to ICP-MS - Part III: The plasma source. In: *Spectroscopy* 16.6, pp. 26–+. ISSN: 00401706. URL: [isi:000169349200003](http://www.isi.com/000169349200003).
- To, Ming Ho et al. (2017). Mechanistic study of atenolol, acebutolol and carbamazepine adsorption on waste biomass derived activated carbon. In: *Journal of Molecular Liquids* 241, pp. 386–398. ISSN: 01677322. DOI: 10.1016/j.molliq.2017.05.037. URL: <http://dx.doi.org/10.1016/j.molliq.2017.05.037>.
- Treybal, R.E. (1981). *Mass-transfer Operations*, 3rd ed., McGraw-Hill. Using tree fern as a biosorbent. *Process Biochem.* In: 40.1, pp. 119–124.
- Vassilev, Stanislav V. et al. (2013). An overview of the composition and application of biomass ash. Part 1. Phase-mineral and chemical composition and classification. In: *Fuel* 105, pp. 40–76. ISSN: 00162361. DOI: 10.1016/j.fuel.2012.09.041. URL: <http://dx.doi.org/10.1016/j.fuel.2012.09.041>.
- Wahlström, Margareta et al. (2013). Acid neutralization capacity of waste – specification of requirement stated in landfill regulations. *TemaNord* 2009:580. Vol. 53. 9, pp. 1689–1699. ISBN: 9788578110796. arXiv: [arXiv:1011.1669v3](https://arxiv.org/abs/1011.1669v3).
- White, L.C. et al. (2003). Removal of arsenic by red mud from contaminated waste water. In: *Proceedings of the TMS Fall Extraction and Processing Conference 2*, pp. 1951–1957.
- Xiong, Zikang et al. (2021). Selective adsorption of Congo red and Cu(II) from complex wastewater by core-shell structured magnetic carbon@zeolitic imidazolate frameworks-8

REFERENCES

- nanocomposites. In: *Separation and Purification Technology* 277, May, p. 119053. ISSN: 18733794. DOI: 10.1016/j.seppur.2021.119053. URL: <https://doi.org/10.1016/j.seppur.2021.119053>.
- Xu, Nan and Yuan Gao (2008). Characterization of hematite dissolution affected by oxalate coating, kinetics and pH. In: *Applied Geochemistry* 23.4, pp. 783–793. ISSN: 08832927. DOI: 10.1016/j.apgeochem.2007.12.026.
- Yu, Kai Ling et al. (2021). Adsorptive removal of cationic methylene blue and anionic Congo red dyes using wet-torrefied microalgal biochar: Equilibrium, kinetic and mechanism modeling. In: *Environmental Pollution* 272, p. 115986. ISSN: 18736424. DOI: 10.1016/j.envpol.2020.115986. URL: <https://doi.org/10.1016/j.envpol.2020.115986>.
- Zouboulis, Anastasios and Konstantinos Kydros (Apr. 2007). Use of red mud for toxic metals removal: The case of nickel. In: *Journal of Chemical Technology and Biotechnology* 58, pp. 95–101. DOI: 10.1002/jctb.280580114.
- Zouboulis, Anastasios I and Konstantinos A Kydros (1993). Use of red mud for toxic metals removal: the case of nickel. In: *Journal of Chemical Technology & Biotechnology* 58.1, pp. 95–101.

Appendix

A Quality control

Table A.1: Quality control of ICP-MS analysis in laboratories CIC (Granada) and CIDERTA (Huelva). Relative differences of the measured concentrations and the standard concentrations.

Element	CIC (ppb)	CIDERTA (ppb)		Standard (ppb)		CIC relative dif (%)		CIDERTA relative dif (%)	
	19-1140-A	19-1140-A	19-1140-B	19-1140-A	19-1140-B	19-1140-A	19-1140-A	19-1140-B	
Ag	42849			51220	50.01	16			
Ba	35759	44935	46.9	51220	50.01	30	12	6	
Bi	51164	40831	43.1	51220	50.01	0	20	14	
Cd	35903	45885	45.5	51220	50.01	30	10	9	
Co	34863	47887	47.4	51220	50.01	32	7	5	
Cr	35141	48500	74.5	51220	50.01	31	5	-49	
Cu	34234	48690	54.0	51220	50.01	33	5	-8	
Ga	33314	45807	46.4	51220	50.01	35	11	7	
In	39087	44524	43.7	51220	50.01	24	13	13	
Li	13476	46593	45.6	51220	50.01	74	9	9	
Mn	35595	47308	47.7	51220	50.01	31	8	5	
Ni	33982	45076	44.8	51220	50.01	34	12	10	
Pb	32357	39327	41.5	51220	50.01	37	23	17	
Sr	35517	45772	47.0	51220	50.01	31	11	6	
Tl	28831	39597	41.9	51220	50.01	44	23	16	
Zn	32063	45886	47.5	51220	50.01	37	10	5	

Table A.2: Quality control of ICP-OES analysis in laboratories CIC (Granada) and CIDERTA (Huelva). Relative differences of the measured concentrations and the standard concentrations.

ICP-OES	CIC (ppb)	CIDERTA (ppb)	Standard (ppb)	CIC relative dif (%)	CIDERTA relative dif (%)
Element	19-1140-A	19-1140-A	19-1140-A	19-1140-A	19-1140-A
Al	39200	49000	51220	23	4
Ca	44230	48000	51220	14	6
Fe	46220	48100	51220	10	6
K	28620	50500	51220	44	1
Mg	45250	47500	51220	12	7
Na	37950	50900	51220	26	1

A QUALITY CONTROL

Table A.3: Quality control of XRF analysis results from laboratory CITIUS (Seville) by comparison with ICP-OES results from CIC (Granada).

	ICP			FRX		
Code	21-1319	22-1111	22-1112	22-1319	22-1111	22-1112
Solid	RM-H	RM-P	DA	RM-H	RM-P	DA
Element	%	%	%	%	%	%
Al	12.4	7.9	0.58	12.3	10.1	0.43
Ca	3.7	0.20	24.7	4.4	0.75	25.3
Fe	13.8	29.7	0.4	15.6	31.5	0.41
K	0.10	0.091	5.0	0.060	0.060	4.2
Mg	0.12		3.8	0.090	0.050	2.9
Mn	0.028	0.036	0.34	0.030	0.070	0.32
Na	5.4	2.8	2.7	8.7	5.0	3.2
P	0.12	0.062	0.84	0.14	0.17	0.95
S	0.41	0.050	0.55	0.59	0.10	0.57
Ti	0.74	0.39	0.081	4.1	3.9	0.14

B Solid wastes characterization

Table B.1: Solid residues composition of mayor elements (%) and trace elements (mg/kg), measured by XRF, ICP-OES and and ICP-M, typical soil values and NGR values.

Solid	RM-H	RM-P	DA	Typical soil	NGR
Code	21-1319	22-1111	22-1112	-	-
Element	%	%	%	%	%
Al	12.3	10.1	0.43	8.2	-
Ca	4.4	0.75	25.3	2.6	-
Fe	15.6	31.5	0.41	3.5	-
K	0.060	0.060	4.2	2.3	-
Mg	0.090	0.050	2.9	1.5	-
Na	8.7	5.0	3.2	2.4	-
P	0.14	0.17	0.95	0.033	-
S	0.59	0.10	0.57	0.062	-
Si	6.6	2.8	1.1	0.31	-
P.C.	12.7	14.0	39.3	-	-
Element	mg/kg	mg/kg	mg/kg	mg/kg	mg/kg
Ag	2.2	2.4	1.2	0.053	-
As	11.9	10.0	24.0	4.8	36
Be	1.3	0.87	0.47	2.1	145
Cd	0.54	0.31	0.71	0.090	25
Co	8.8	2.1	4.7	17.3	24
Cr	540.1	1500.3	42.7	92.0	10020 ¹
Cu	136.9	62.0	262.3	28.0	595
Hg	0.28	0.000	0.0021	0.050	31 ²
Ni	26.3	16.4	37.4	47.0	1530
Pb	100.0	200.0	100.0	17.0	275
Th	100.9	67.3	0.90	10.5	-
U	14.6	9.2	0.66	2.7	-
Zn	100.0	1500.0	500.0	67.0	10000

C Isotherm adsorption models

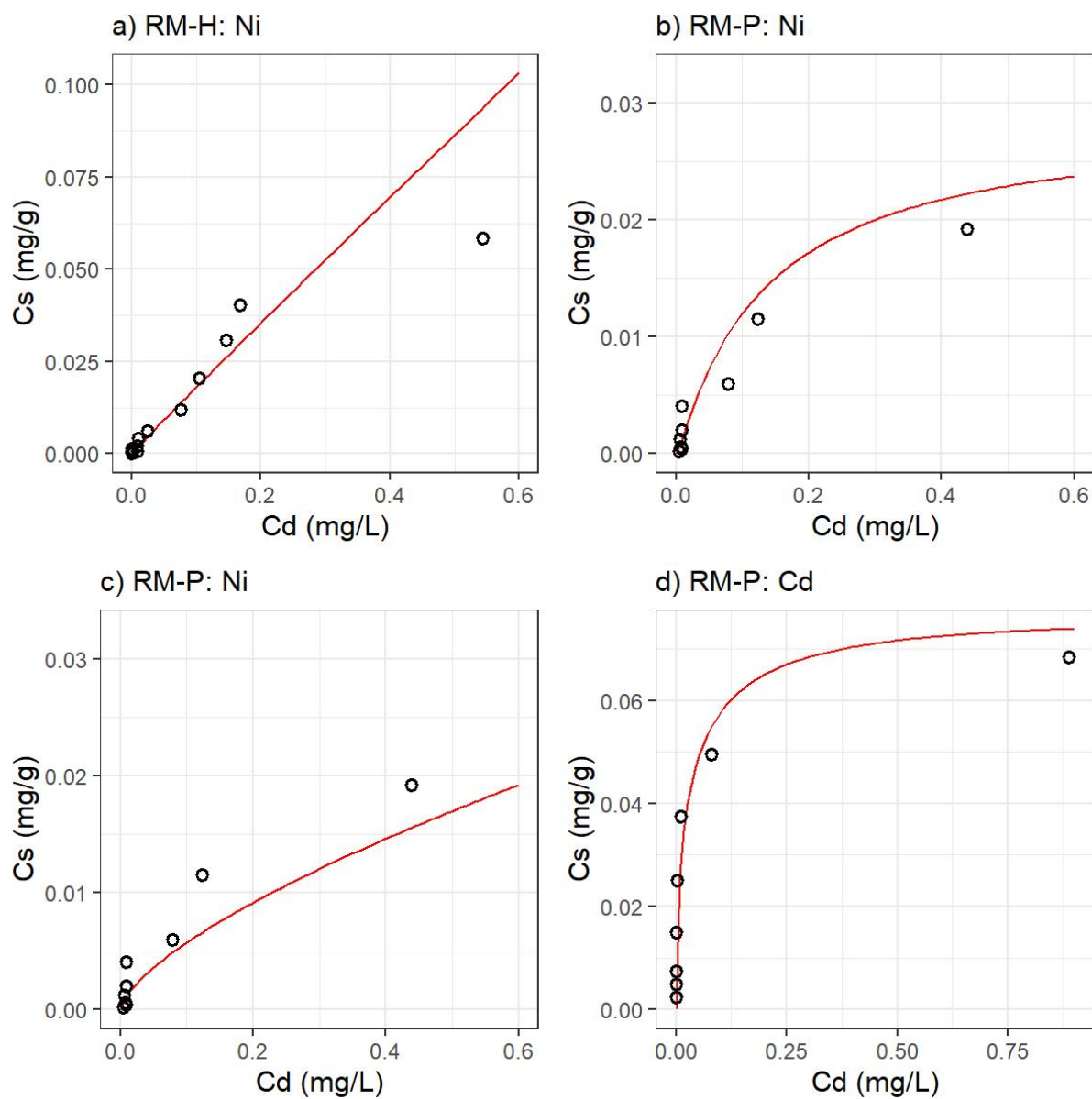


Figure C.1: Best fit of Ni and Cd isotherms to Freundlich model (a and c) and DR model (b and d).

¹10000 mg/kg for Cr(III), 20 mg/kg for Cr(VI)

²6 mg/kg for elemental Hg, 25 mg/kg for inorganic Hg